Evaluation of Aerogel Composite Insulations by Characterization and Experimental Methods

By

Chotangada Gautham Somana

B.Eng., R.V College of Engineering, Bangalore, India, 2012

A thesis submitted to the graduate degree program in the Department of Civil, Environmental, and Architectural Engineering and the Graduate Faculty of the University of Kansas in partial fulfillment of the requirements for the degree of Master of Science in Architectural Engineering.

_____
Mario A. Medina, Ph.D., P.E., Chairperson

_____
Robert L. Parsons, Ph.D., P.E., Member

_____
C. Bryan Young, Ph.D., P.E., Member

Date Defended: _____

The thesis committee for Chotangada Gautham Somana
certifies that this is the approved version of the following thesis:

Evaluation of Aerogel Composite Insulations by Characterization and Experimental Methods

_____
Mario A. Medina, Ph.D., P.E., Chairperson

Date approved: _____

ABSTRACT

The purpose of this thesis was to study aerogel blankets as building insulation. These blankets may potentially have lower thermal conductivities than conventional insulations. As such, two types of aerogel blankets were characterized and evaluated experimentally.

This thesis documents the steps that were taken to analyze and understand the thermal performance of aerogel blankets for building insulation application. The results were obtained over one summer season under Midwestern U.S.A. weather conditions.

It was found that the aerogel blankets reduced the peak heat fluxes by up to 22% and the daily heat flows by up to 35% when compared to a non-insulated wall. The aerogel blankets produced an average of 5% reduction in peak heat flux and an average daily heat flow reduction of 16% when compared to conventional insulation. The aerogel blankets did not perform as well as aerogel monoliths and showed marginal differences in heat flux reductions when compared to conventional insulation.

It was concluded that the macro structure of the aerogel composites, quantity of aerogel, and granular size can influence the thermal conductivity of the blankets. Methods by which composite aerogels may be further developed and researched were noted.

Acknowledgement

I would like to express my deepest gratitude to Prof. Mario A. Medina for giving me this opportunity to research under his guidance. His suggestions and advice have been priceless. His mentorship has taught me patience and has allowed me to develop into a goal oriented researcher.

I express my warm thanks to Prof. Robert L. Parson and Prof. C. Bryan Young for their participation in my committee. Their constructive comments and friendly advice have been helpful.

I thank my co-researcher Dr. Kyoung Ok Lee for her ever-present guidance. Her guidance on experimental procedures has been pivotal to this research. I would also like to thank Arun P. Kuppusamy for his timely help during the duration of this research.

I am thankful to Dr. Prem Thapa for sharing his expertize during imaging and microscopy and Felipe B. Nishida, who helped me during my experimental setup at M2SEC.

A special thank you to my parents and brother, who have always been supportive of my work.

C. Gautham Somana

TABLE OF CONTENTS

LIST OF FIGURES

LIST OF TABLES

Nomenclature

c	Speed of light in a vacuum (3×10^{8} m/s)
D_P	Mean pore diameter of a porous medium (m)
$e(T)$	Extinction coefficient (m^{-1})
k_S	Solid thermal conductivity (W/mK)
k_G	Gaseous thermal conductivity (W/mK)
k_{GA}	Thermal conductivity of air (W/mK)
k_R	Radiative thermal conductivity (W/mK)
k_{eff}	Total effective thermal conductivity (W/mK)
Kn	Knudsen number
l_g	Mean free path of a gas (m)
λ_{MAX}	Wavelength at which radiation is maximum (m)
ρ	Density of aerogel (kg/m^3)
Ø	Porosity of the aerogel
σ	Stefan-Boltzmann constant (5.68×10^{-8} W/m^2K^4)
n	Index of refraction
T	Absolute temperature (K)

v Speed of light through the material (m/s)

D_{par} Aerogel particle diameter (mm)

D_V Minimum inter-granular distance (mm)

Chapter 1
Introduction

As the consumption of energy increases rapidly, especially in developing countries like India and China, energy conservation technologies and efforts continue to gain momentum. The building sector consumes more than one-fourth of the total energy worldwide. This amount is expected to increase in the coming years, as urbanization becomes the norm around the world [1]. The problems associated with an increase in energy production are two-fold: 1) the finite nature of conventional energy resources and 2) the adverse effects of generating useful energy; including pollution and global warming.

The burning of fossil fuels is a major contributor of carbon dioxide, methane, and other pollutants which aggravate greenhouse effects. It is estimated that more than 70% of all worldwide electrical energy is produced using fossil fuels [2]. Fossil fuels, namely, petroleum, coal, and natural gas are a finite resource. They are a dense form of energy and take millions of years to produce. Based on proven-reserves of fossil fuels and at the current rate of consumption these may last for about 100 years [3]. Global warming is an issue of concern. For example, in the United States, ambient air temperatures recorded for the July 2011 through June 2012 period exceeded previously collected temperatures [4]. Global warming is seen as an impact of the increase in levels of greenhouse gases (e.g., CO_2, N_2O, CH_4, and others).

There is a growing shift in attitude towards reducing energy consumption as opposed to meeting its demand. By using thermal insulation in buildings, primarily in

high energy consumption applications like space heating and cooling, the burning of fossil fuels can be reduced, which can assist towards reaching the goal of having buildings that are low energy consuming. Currently, space heating and cooling, together with domestic hot water are estimated to account for roughly half of all global energy consumption in buildings [5]. In an effort to cut down on energy gains and losses through building enclosures, efficient building thermal insulation has been considered. To make traditional building insulation materials reduce the most heat transfer across building enclosures, thicker walls would be needed in which more layers of insulating material would be used. This would reduce usable work and living spaces and is often not as effective as conceived, largely because of the compression created by adding extra insulation.

Aerogel since its conception in the 1930's has been a potential solution to the heat gain and loss problem between systems and their environments. Having a thermal resistance a number of times that of its traditional counterparts [6], it can lead to thinner insulation layers. In addition, being lighter, aerogel-containing insulation becomes easier to install and to handle in buildings. Although in the development of aerogels a majority of its cost have been reduced by switching to cheaper production methods and materials, for aerogels to be viable as a building insulation it must be commercialized and produced on a larger scale. The manufacturing process of silica aerogels is explained in section 1.2.2.

An evaluation of thermal enhancement of building enclosures using aerogels is required. This research project addresses the use of aerogels as an effective and more flexible thermal insulation.

1.1 Thermal insulation

Heat transfer occurs when energy is transmitted as a result of temperature difference. Humans have for time immemorial used materials to protect themselves from the environment in the form of clothing and shelter. The use of material in enclosures, as a separate insulating material is not a new concept, often in rural areas around the world, straw, mud, cotton and wool are used as thermal insulation. There are a number of materials that are in common use in the building industry and some are listed in Table 1.

Table 1
Properties of commonly used thermal insulations [7].

Form	**Material**	**Density (Kg/m^3)**	**Thermal (W/mK)**
Blankets: Batts or rolls	Fiberglass	12-56	0.033-0.04
	Rockwool	40–200	0.037
	Polyethylene	35–40	0.041
Loose-fill blown-in or	Fiberglass	10–48	0.03-0.038
	Rockwool		0.004
	Cellulose	24–36	0.046-0.054
	Perlite	32–176	0.004-0.006
	Vermiculite	64–130	0.063-0.068
Rigid Board	Fiberglass	24–112	0.032-0.035
	Expanded Polystyrene	16–35	0.037-0.038
	Extruded Polystyrene	26–45	0.03-0.032
	Polyurethane and Polyisocyanurate	40–55	0.023
	Vermiculite	64-130	0.063-0.068

Sprayed-in- place	Cellulose	24–36	0.046-0.054
Foamed in place	Polyurethane and Polyisocyanurate	40–55	0.023
Reflective systems	Aluminized thin sheets		Reduces only radiant heat
	Ceramic coatings	1.25	Radiation control

Note: Thermal conductivity varies with material density and thickness as well as temperature and moisture content.

The idea of using thermal insulation as a building enclosure layer is to save on energy consumption by preventing heat gain or loss and maintaining constant indoor air and surface temperatures. This is possible by the use of materials that have low conduction values. Thermal transport by conduction is the result of atomic vibrations. In general, materials that are denser, having a closer lattice structure, are better thermal conductors. Convection is the heat transfer by a combination of conduction and the flow of a fluid. A key feature of thermal insulation is its ability to reduce convective flows by restricting the motion of air within building enclosures. Within buildings, radiation thermal transport is the result of emitted energy in the infrared region of the electromagnetic spectrum.

Most kinds of thermal insulations work in a similar way. They trap air or other gases that have low thermal conductivities, minimize convective flow, and hinder radiation from being transmitted by scattering or absorbing it. In the building industry, thermal insulation is rated by R-value. This is a measure of thermal resistance which in turn is a function of material thermal conductivity and has units of m^2K/W. For illustration purpose, Fig. 1 shows a wall section, and its corresponding components and thermal variables.

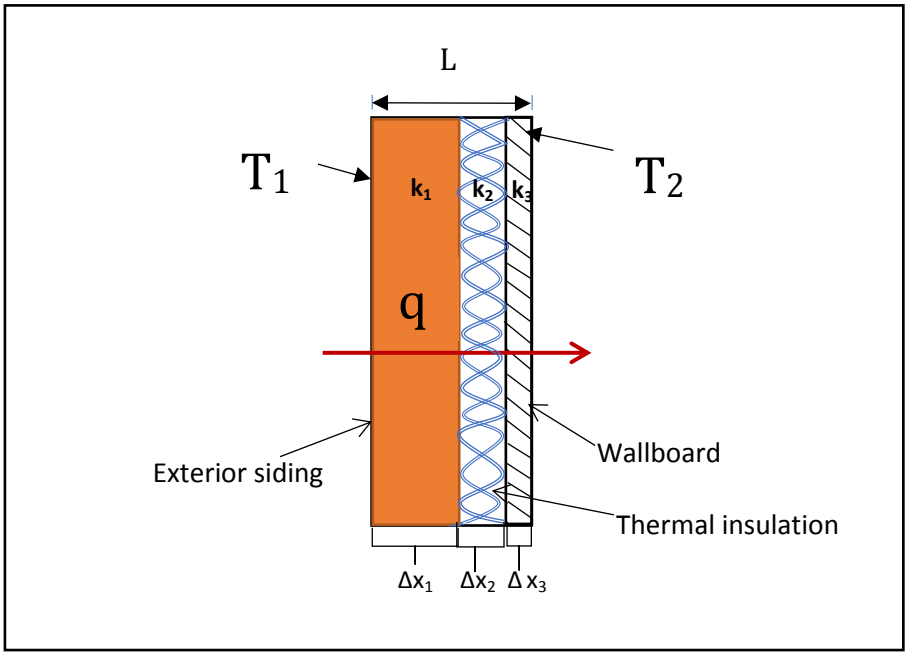

Fig. 1. Wall section showing its components and variables.

In Eq. (1.1), Δx is the width of the wall components and k is the thermal conductivity (W/mK). In Eq. (1.2) ΔT is the difference between the exterior wall surface temperatures T_2 and T_1, R_W is the sum of the resistances of the wall layers, and q is the heat flux through the wall (W/m^2).

$$R_i = \frac{\Delta x_i}{k_i} \tag{1.1}$$

$$q = -\frac{\Delta T}{R_W} = \frac{T_1 - T_2}{R_W} \tag{1.2}$$

The total R-value of the wall in Fig. 1 is given by Eq. (1.3).

$$R_W = \frac{\Delta x_1}{k_1} + \frac{\Delta x_2}{k_2} + \frac{\Delta x_3}{k_3} \tag{1.3}$$

The trapped gas is the limiting factor to the R-value of the insulation. That is, most air based insulations cannot exceed the R-value of still air. Polymer-based foams, like polystyrene and polyurethane, also trap gases in their cells, including air and fluorocarbons. Fluorocarbon gases have higher R-values than air [7]. An efficient insulation product should not only be judged by its R-value, but also its cost, weight, ease of application, and its availability.

1.1.1 Concept of superinsulation

Superinsulators are materials that can achieve conductivity values of less than 0.02 W/mK. Most traditional building materials cannot achieve this value [7]. In buildings, the most common way in which the higher thermal conductivity of enclosing materials is compensated for is by increasing wall thickness. Still air is considered a good insulator. However, it has a minimum conductivity of 0.026 W/mK [8]. This demarcates a limit for air as an insulator. Different materials that reach these low thermal conductivities often are the result of different thermal mechanisms.

For example, vacuum insulated panels (VIP) can achieve a thermal conductivity as low as 0.003-0.004 W/mK. The vacuum in these panels prevents gaseous conduction

and convection across the panel. VIPs, however, come at a very high cost and require extra care when handled [9].

Aerogels can achieve low thermal conductivity values such that they could be considered superinsulators [10]. Despite the fact that aerogels work by trapping air they can approach a lower thermal conductivity than air. Details of the heat transfer mechanisms of aerogels are given in section 1.2.3.

1.2. Aerogels

Aerogels comprise of a large variety of ultra-low density porous solids. The most common aerogels are made of carbon and silica. Fig. 2 shows a photograph of silica aerogel. The sizes of the pores formed in aerogels are in the nanoscale range and are open in structure. Aerogels are also considered to be the lightest solids in existence. Most commercially-available aerogels used for thermal insulation are silica aerogels. Silica aerogels are often blue in color. This is an effect of Rayleigh scattering. The wavelength of blue light is around 475 nm, which is close in size to typical networks of pores within the aerogel. These act as scattering centers for the wavelength of blue light. Rayleigh scattering is the same effect that causes the sky to appear blue [11].

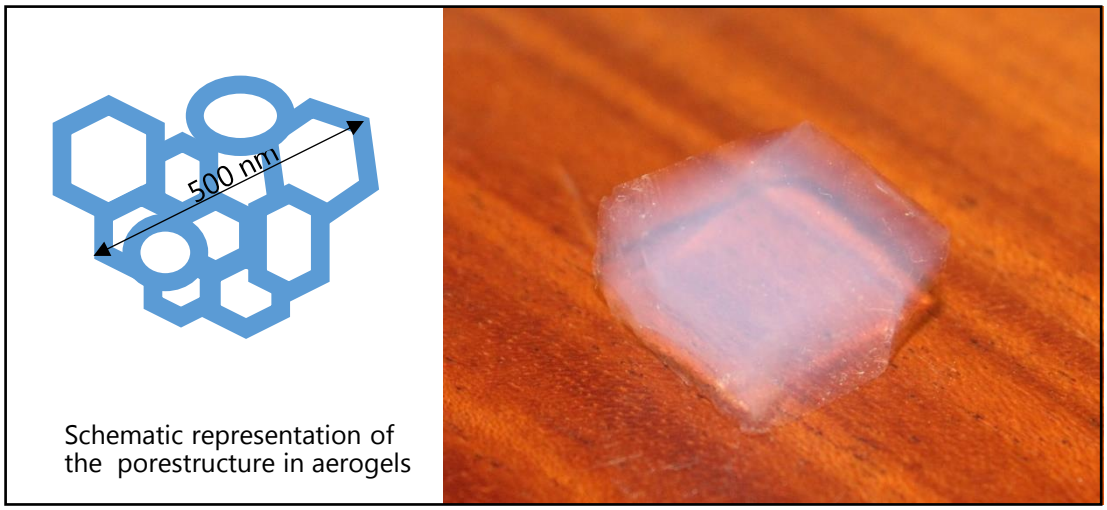

Fig. 2. Silica aerogel.

For building applications, some desirable characteristics of aerogels include their low thermal conductivity, high transparency, and low density. Aerogel insulation is available in the form of flexible blankets, boards, and transparent films. Some general properties of silica aerogels are given in Table 2. These properties qualify them for use in a number of applications. The properties of silica aerogels differ depending on materials, additives and synthesis techniques.

Table 2
Typical properties of silica aerogels [5,12].

Property	**Value**
Apparent density	0.03–0.35 g/cm^3
Internal surface area	600–1,000 m^2/g
Percent of solids	0.13–15%
Mean pore diameter	~20 nm
Primary particle diameter	2–5 nm
Refractive index	1.0–1.08
Coefficient of thermal expansion	2.0–4.0 × 10^{-6} K^{-1}
Dielectric constant	~1.1
Sound velocity	100 m/s
Thermal conductivity	<0.02 W/mK

Hydrophilic compounds have the tendency to attract water because of the presence of polar groups that have unbalanced electrons. Conversely, hydrophobic compounds repel water and have non-polar groups. Fig. 3 shows an image of silica aerogel dust as was taken under a scanning electron microscope (SEM) at 80X magnification. The aerogel dust particles show cracked and uneven surfaces. These cracks are potential entry points for water vapor. Water vapor by itself does not damage the nanostructure of the aerogel. However, upon condensation the surface tension of water may collapse the nanostructure of hydrophilic aerogel, rendering it ineffective [13]. Moreover, these cracks form breaks in the thermal insulating body of the aerogel and can prove detrimental to the thermal insulating characteristics of the aerogel.

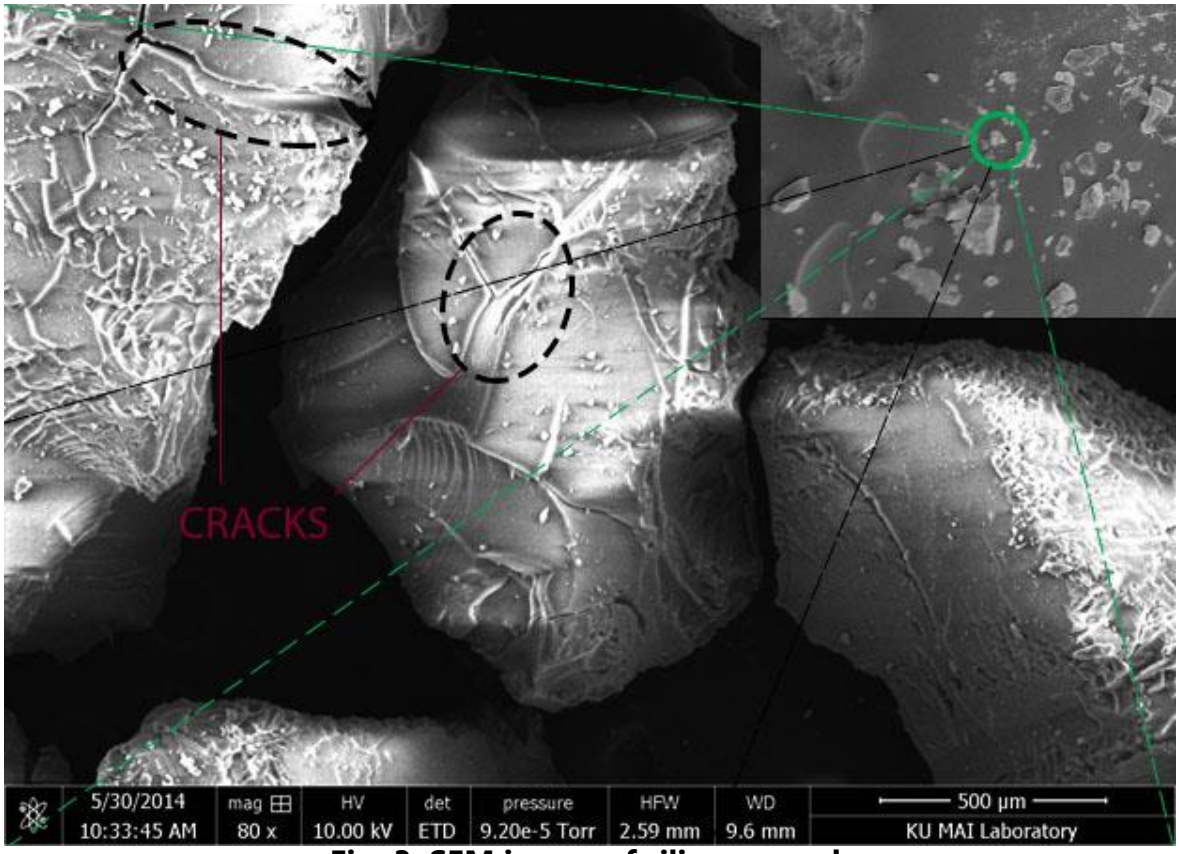

Fig. 3. SEM image of silica aerogel.

For aerogels, their primary drawbacks are their cost, shrinkage, and hydrophilic nature. Hydrophilic aerogels have Si-OH groups which undergo strong bonding with water that result in the destruction of their nanostructures [5]. However, it is possible to prepare hydrophobic aerogels by the use of additives and surfactants. Jung et al. [14] prepared a hydrophobic silica aerogel by doping silica with silicon dioxide nanoparticles using ambient pressure drying.

1.2.1. History of aerogels

Kistler [15] noted in 1931 that aerogels had a remarkably low thermal conductivity. This aerogel's main raw material was sodium silicate. The first recorded commercial marketing of aerogels was in the 1940's by Monsanto Corp. which used Kistler's silica aerogel and marketed it as Santocel®. It was made for application as a thickening agent in toothpastes, cosmetics, thermal insulation in freezers, and as a filter in cigarettes. This first attempt at the commercialization of Kistler's silica aerogel was a failure because of high production costs [15]. It can be noted that at the time aerogel technology was in its nascent stage and were produced based on Kistler's original production method which was slower and relied on the high temperature supercritical drying of aerogel.

Kistler's aerogel was improved by using tetramethylorthosilicate (TMOS) instead of sodium silicate. This improved method produced aerogel in a shorter time and gave rise to the modern day sol-gel process [16]. Over the years different precursors and solvents have been used, which have led to the manufacturing of aerogels in a much safer manner [17].

1.2.2. Manufacturing of aerogels

Aerogels can be produced through many variations in technique. However, essentially there are three steps involved; the sol-gel process, aging and drying. The sol-gel process involves the synthesis of a solid in a liquid medium at a temperature less than 100 °C. It involves the use of a precursor (normally an oxide or hydroxide), solvents, and reactants. Solids are formed by polymerization and can be either organic

or inorganic. The microscopically dispersed particles form branches and interlink with each other forming a 3-D network while still in the solvent which is what forms the gel. The first synthesized silica aerogel used sodium silicate as a precursor, water as a solvent, and hydrochloric acid as a catalyst. The use of sodium silicate was subsequently replaced by organic monomers which proved to be less laborious, giving rise to the modern sol-gel process [18]. The sol-gel process can be replicated using a number of materials and reactants, which lends different properties to the aerogel.

Silica aerogel was manufactured using rice hull ash, instead of organic silicon monomers, such as tetramethylorthosilicate (TMOS), tetraethylorthosilicate (TEOS), and polyethoxydisiloxane (PEDS), which are generally selected as sources for silica. Rice hull ash, which is a byproduct of the rice industry, is rich in silica and allows for more economical production of silica aerogel [19].

When the gel visibly spans the container it is known as gel point. After the gel point is reached some time must be given for all the unreacted elements to condense and form. This is done by leaving the gels untouched for 48 hours. This process can be expedited by soaking the gel in 1:1:1 ratio of water, alcohol, and the original solution at a pH between 8 and 9 [20].

The next step involves the drying of the wet gel. The key to this process is the vaporization of the liquid component without putting strain on the aerogel skeleton. This was initially made possible by supercritical drying. A supercritical fluid is a fluid whose phases at its critical temperature and pressure are indistinguishable. This procedure involves the removal of the supercritical fluid present in a gel by exposing it

to pressure and temperature exceeding its critical pressure and temperature. This leaves only the solid framework having a high pore volume [21].

Alternatively, aerogels can be also be formed at ambient temperatures by the use of liquids that evaporate at ambient temperature and pressure [22]. This has allowed aerogel to become more commercially viable as ambient drying proves to be cheaper than supercritical drying.

1.2.3. Heat transfer mechanisms in aerogels

In a simplified manner, heat transfer in organic monolithic aerogels is the sum of the conductivity through the solid backbone (k_S), the gaseous conductivity through the nanostructure (k_G), and the radiative thermal conductivity (k_R) [23]. Silica aerogel is assumed to be isotropic resulting in a heat transfer that is independent of direction. Therefore, the thermal conductivity is given by Eq. (1.4).

$$k_{eff} = k_S + k_G + k_R \tag{1.4}$$

To present the heat transfer mechanisms in aerogels, silica aerogel was used because this is the most widely researched aerogel to date. Fig. 4 represents the nanopore structure of aerogel. In Fig. 4 the thermal pathways in aerogel are depicted.

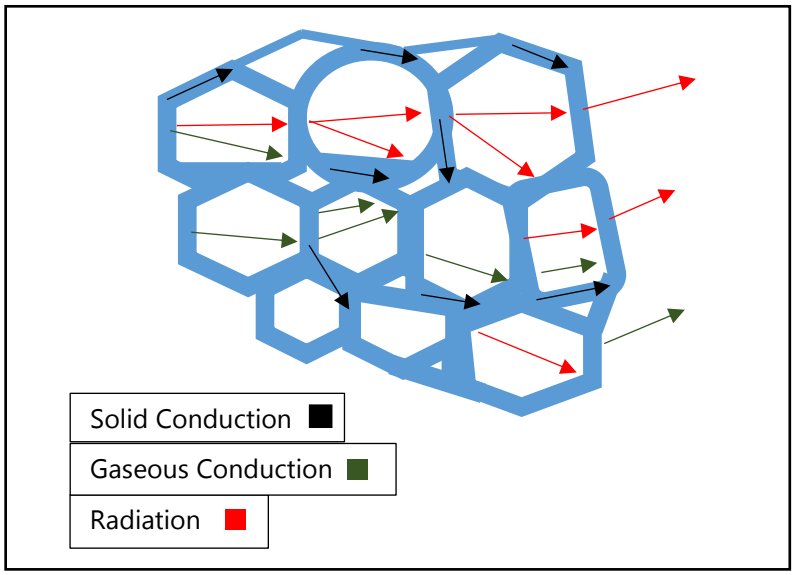

Fig. 4. Thermal pathway through aerogel nanopores.

When x-rays are incident on an object they are scattered in different ways according to their pore distances, shape and size of the macromolecules. This range of data gives a glimpse of the macrostructure of a material. The existence of the solid backbone of silica aerogel has been shown to exist by small angle x-ray scattering measurements [24]. In the scanning electron microscope image shown in Fig. 5, the branched structures of silica aerogel are observed (shown in white), as well as pores (shown in black), sizes ranging from in between 10 nm to 200 nm. This random network creates silica aerogel's unique nanopore structure.

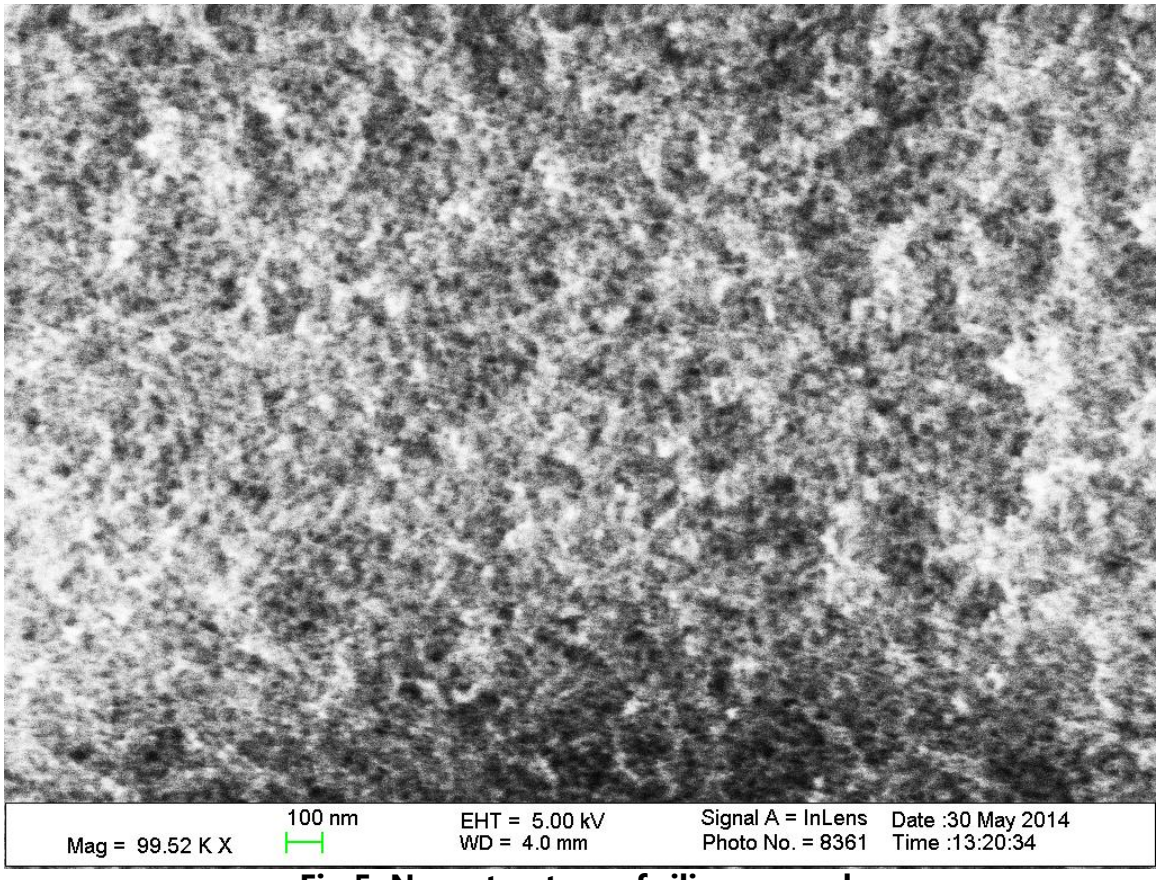

Fig.5. Nanostructure of silica aerogel.

Conduction through the solid backbone depends on its material and density. Silica (SiO_2) has a high thermal conductivity when compared to what is expected of an insulating material. However, the reduced solid content and its terminating lattice like structure are the restricting factors for conduction through the solid. Solid conductivity can be calculated by Eq. (1.5) [25].

$$k_S = C\rho^{\mu} \tag{1.5}$$

Where C is a constant that depends on the interconnectivity of the 3-D network, ρ is the density of the aerogel, and μ is a constant found to be around 1.5.

The mean free path is the average distance travelled by particles between successive collisions. The mean free path of air is 7.46×10^{-3} mm [26]. This means that one air molecule will travel 7.46×10^{-3} mm before hitting another air molecule and transferring energy to it. The Knudsen number (Kn) takes into account the mean free path of a gas (l_g) and the mean pore diameter of a porous medium (D_P). The relationship between l_g and D_P is represented in Eq. (1.6). The mean pore diameter can be approximated from the density and the uniformity of the aerogel nanostructure (ϒ) as is shown in Eq. (1.7).

$$Kn = \frac{l_g}{D_P} \tag{1.6}$$

$$D_P \ \alpha \ \frac{1}{P^{\Upsilon}} \tag{1.7}$$

The Knudsen number along with the porosity of the aerogel (ø), the thermal conductivity of air (k_{GA}), and β, which is a parameter that represents the energy transfer between the gas and the limiting structure of the aerogel nanostructure, can be used in the Knudsen Eq. (1.8) to find the gaseous thermal conductivity of aerogels [27].

$$k_G = \frac{k_{GA}\,ø}{(1+\beta Kn)} \tag{1.8}$$

In aerogels, smaller pore diameters (D_P) increase the Knudsen number which in turn reduces the gaseous thermal conductivity. The reason for this is that air has a free mean path similar to the size of the nanopores which drastically reduces gaseous molecular collision, which in turn reduces heat transfer [26,28]. The air molecules collide with the solid backbone instead. This prevents a proper convection from developing and allows aerogel to develop a gaseous conductivity far less than that of air.

Heat transfer can occur by successive thermal re-radiation through the aerogel or by passage through translucent/transparent aerogel by radiation. The nature of heat transfer through aerogel is dependent on its optical thickness or measure of transparency [29]. The radiation conductivity is represented by Eq. (1.9). Where, n is the index of refraction, σ is Stefan-Boltzmann constant, T is the absolute temperature, e(T) is the extinction coefficient and P is the density of the aerogel [23].

$$k_R = \frac{16}{3}\frac{n^2\sigma T^3}{(e(T)P)} \tag{1.9}$$

The radiative conduction is sensitive to changes in temperature (T) and the refractive index (n). This is why the thermal conductivity of aerogels is not constant and change as temperature is increased [6]. The refractive index is given in the equation below.

$$n = \frac{c}{v} \tag{1.11}$$

In this equation, c is the speed of light in a vacuum and v is the speed of light through the material. The refractive index of silica aerogel is 1.0–1.08, which is close to that of air [5]. However, imperfection in its structure may increase the refractive index of aerogels. Within a medium, radiation can be transmitted, scattered and/or absorbed. The extinction coefficient is a measure of how well a material impedes the movements of radiation of a given wavelength through its body. Its calculation is comprised of the materials absorption and scattering capabilities which are dependent on pressure, temperature and wavelength. In aerogels, because of the relatively small pore diameters (<100 nm) in comparison to the size of near infrared wavelengths (>800 nm) scattering does not take place. Furthermore, pore size is responsible for allowing wavelengths in the visible spectrum to be transmitted while preventing the transmission of those in the infrared radiation range from being transmitted [30]. These properties make it ideal for application to windows as it blocks heat in the form of infrared radiation and allows the passage of light in the visible range. It also prevents the conduction of heat through the window.

Often, additional substances known as opacifiers are added to improve the absorption properties of the aerogel. Carbon black and titanium dioxide added in

limited quantities can increase the extinction coefficient of the aerogel [5,30]. At higher temperatures, radiation heat transfer is a significant mode of heat transfer in aerogels when compared to conduction and convection [31]. This is because at higher temperatures radiation is propagated in smaller wavelengths and also at elevated temperatures the extinction coefficient of materials, which is lower, makes disruptions in heat transfer fewer and renders aerogels less effective [32]. However, the higher temperatures required to cause significant changes in thermal properties are unlikely to occur in typical building situations.

Monolithic aerogels have the unique advantage of having pore sizes hundreds of times smaller than conventional insulations. The equations provided in this section are applicable to porous insulations that work by trapping air or other gases. In insulating materials, gaseous conduction is the significant mode of heat transfer. Gaseous conduction is directly related to pore size as shown in Eqs. (1.5) and (1.8). The reduction of gaseous conduction in highly porous materials is known as the Knudsen effect, which is seen in aerogel monoliths. However, this effect is negligible in materials with pore sizes greater than 0.01 mm (conventional insulations). For example, fiberglass which has a pore size between 10 to 100 μm, has a thermal conductivity of about 0.040 W/mK. Typical silica aerogels have a thermal conductivity of 0.017 W/mK. This is what eventually makes aerogel monoliths better thermal insulators than conventional insulations.

1.2.4. Aerogel application areas

As a material, aerogel has a number of useful properties as illustrated previously in Table 2. These properties can be modified based on the sol-gel process, drying techniques, and use of modifiers. In Table 3, possible applications are listed.

Table 3
Scope of aerogel applications [33].

Property	Features	Applications
Thermal conductivity	High insulating properties Wide range of temperature	Architectural and appliance insulation, portable coolers, transport vehicles, pipes, cryogenic, skylights, space vehicles, probes and casting molds.
Density or porosity	Lightest synthetic solid Homogeneous High specific surf. Area	Catalysts (e.g. automotive CO oxidation by O_2), absorbers (e.g. for oil spills), sensors for different airborne compounds, fuel storage, targets for ICF [(1)].
Optical	Low refractive index solid Transparent/translucent	Cherenkov detectors[(2)], lightweight optics, and special effect optics.
Acoustic	Low sound speed	Radars, speakers, and sound insulation.
Mechanical	Elastic Lightweight	Energy absorber and substitutes for plastics.
Electrical	Low dielectric constant[(3)] High dielectric strength[(4)]	Spacers for vacuum electrodes and capacitors.

Notes:
(1) Inertial confinement fusion (ICF) is a type of fusion energy that is formed by compressing and heating a target.
(2) When a particle passes through a material at a velocity greater than that of the speed of light through the same medium, it emits light as Cherenkov radiation that can be used to identify the particle.
(3) Dielectric constant is a measure of the permeability of a material to electricity. Materials with lower dielectric constants allow capacitors to store more charge.
(4) The amount of electrical energy that a material can withstand without its insulating properties breaking down is known as dielectric strength.

The apparent density of silica aerogel, 0.03–0.35 g/cm^3 [12], is certainly much lower than that of conventional insulations. The low aerogel weight would facilitate the transport and installation of prefabricated wall panels. Recently, aerogel technologies have been used to manufacture small handheld gadgets used for telecommunications because of its strong mechanical and low weight properties. The weight of such gadgets has been reduced by about one-half of their weight when polymers were used [34].

Of particular interest to the field of building enclosures is the possible multipurpose use of hydrophobic aerogels. For example, a flexible cryogenic insulation blanket is an aerogel blanket with an integral barrier that serves as a sound, thermal and water vapor barrier and is commercially available for building enclosure use [46]. The optical and thermal nature of silica aerogel allows it to be used as an effective glazing on glass [35]. Many contaminants are released in the interior of a building envelope, from water, paints, and organic solvents. Aerogels made of metal oxides are capable of acting as air filters, removing airborne contaminants that may exacerbate problems such as asthma and allergies [34].

1.3. Research Objectives

The world energy consumption is on the rise. It is forecasted that the energy usage from 2010 to 2040 will increase by approximately 56%. A majority of this energy will come from coal, natural gas and liquid fuels [1]. This exacerbates the already aggravated global warming problem. Furthermore, lack of useful energy in some areas around the world could lead to social and economic disasters. Studies show that power plants require more than 12 times the investment per generated kilowatt-hour than avoiding the use of the same kilowatt-hour by using thermal insulation. This accentuates the importance of finding suitable and efficient insulations [36].

Traditional thermal insulation of the same effective thermal resistance is several times thicker and heavier than superinsulations like aerogel. This increases in multilevel buildings. Moreover, traditional thermal insulations have reached their limit in thermal resistance. This calls for testing materials that can be produced sustainably and that will bring building enclosures to a higher plane of performance.

The main research objective is to evaluate whether an aerogel blanket is an effective and practical thermal insulator when applied to buildings. The primary obstruction to the commercial implementation of aerogels is production costs. As recently tested manufacturing methods and material move into large scale production, it is a matter of time before aerogels become more viable for use in the building industry.

Chapter 2
Literature review

Silica aerogels are a thermal insulating material with a high potential, which have made their way into the building insulation industry. Despite silica aerogels existing for more than 75 years, studies with respect to their use as an insulating material in buildings were not made until recently. This is because of a number of advances in their production that has allowed them to become a more viable and of practical use in buildings [12,14,16,19,22].

Aerogels were first synthesized by Kistler [26,28], who used sodium silicate and the process of supercritical drying to produce aerogels. He extensively studied its properties. He measured the heat conductivity of aerogels containing three different gases at various pressures. Based on kinetic theory he found the relationship between the heat conductivity, mean free path of gas molecules, and pore size. In his later work he went on to explain how heat conductivity can be used to find the density of silica aerogel.

Fricke [16,23,27,34,36] published many papers on aerogels but in particular, related to their thermal resistive properties. He showed the dependence of aerogel conductivity on gas pressure. The lowest pressures showed conductivity reaching into superinsulation values of 0.01 W/mK. He demonstrated the use of aerogel as a suitable thermal insulation material by examining thermal transport in monolith and granular aerogels with regard to gas pressure, temperature, boundary emissivity, and external load [37].

Hrubesh [39] of the Lawrence Livermore National Laboratory, along with his team produced the world's lightest solid which had a density of 0.003 g/cm^3. He consequently published his paper under the name of "Aerogels: The World' s Lightest Solids." His work with regard to aerogels extended to optics, thermal properties, and synthesis. As early as 1998, Hrubesh et al. conducted surveys on the possible applications of aerogels stating clearly their possible use in the building industry.

Ruben et al. [40] studied the nanostructure of silica aerogels which gave greater detail on techniques usable to characterize aerogels. This included properties such as surface area, pore sizes, and connector sizes. The characterization of aerogels is often seen as difficult because of its minute pore sizes.

Aerogel insulation per square foot is considered to be on the costlier side of available thermal insulations. However, analyses indicating the cost effectiveness of aerogels with respect to R-value have been conducted. Carlson et al. [42] showed that aerogels made from sodium silicate were cheaper than fiberglass insulation per R-value per unit length. Their work on cost analysis included a detailed breakdown of all reagents involved in aerogel production and its associated cost. Koebel et al. [5] researched aerogels as a thermal insulation in buildings. They reiterated the effectiveness of aerogels as a thermal insulation and proceed to analyze their viability. The cost per unit volume of aerogels in 2020 may reduce to one-half of its cost in 2009. This cost reduction, coupled with savings in floor space, makes aerogels a more attractive thermal insulation option, especially for retrofits.

Aegerter et al. [5] produced one of the first handbooks related to aerogels. This handbook gave in detail the manufacture, application and properties of most types of aerogels. According to the handbook, organic or organic-inorganic aerogels could eliminate problems associated with traditional aerogels such as mechanical strength, environmental problems, and synthesis.

Advances in manufacturing have also helped reduce these costs. Tewari et al. [22] successfully used ambient temperature supercritical drying by replacing the alcogel with liquid CO_2. This eliminated the need for supercritical drying chambers to sustain high temperatures and pressures. The drying time was also reduced to about 8 hours. Alternate materials for the synthesis of aerogels were also introduced. Table 4 shows the cost sensitivity to different precursor materials for aerogels. One board foot is equal to 30.48 cm × 30.48 cm × 2.54 cm.

Table 4
Aerogel costs [42].

Material	Aerogel cost ($/ board foot)
TMOS	7.91
TEOS	4.15
Sodium silicate	0.63
Resorcinol--formaldehyde (RF)	1.34
Phenol-formaldehyde (PF)	0.42
RF:PF (50:50)	0.89
Melamine-formaldehyde	1.14
Phenolic-furfural	0.73

Tang et al. [19] making use of rice hull ash, a byproduct of the rice industry, synthesized silica aerogel. The aerogel produced by supercritical CO_2 drying was shown to have a density and pore volume size similar to conventional produced TEOS silica aerogel.

Nguyen et al. [41] made use of recycled waste paper to produce cellulose aerogels. Although, it was made to work as an absorbent, this cellulose aerogel showed a low thermal conductivity. Thermal conductivities of 0.029–0.032 W/mK, were recorded. These alternate production techniques reduced costs and in a larger scope were more sustainable. Many of the reagents used in conventional aerogel production (e.g., resorcinol, formaldehyde) are toxic.

A large amount of research was carried out on aerogels for use as a translucent/transparent window glazing. Reim et al. [31] used granular silica aerogel trapped in between two glass panes. This construction achieved a low conductance value of 0.5 W/m^2K for a thickness of only 50 mm. Aerogel insulation glazing was shown to be more effective than a triple pane window.

Producing large monoliths of aerogel is a difficult proposition; it is easier to produce granular aerogel as it fractures easily during manufacture. However, granular aerogel does not perform as well as a monolith because of increased gaseous phase conductivity in the inter-granular region. Smith et al. [43], having identified the problem, produced aerogels with a density of 90–100 $kg/m^3$and a granule size in the 90–250 μm range. These aerogel granules, because of their ability to occupy smaller spaces, performed similar to that of the aerogel monolith at ambient pressure and in a vacuum.

The co-heating test methodology is an experimental method to determine heat loss through a building enclosure and entails plotting heat loss from thermal transmission and infiltration through the building enclosure against variations between a constant indoor temperature and weather dependent outdoor temperatures. Cuce et al. [44] retrofitted one of the rooms in a test house with silica aerogel blankets and proceeded with testing it using a co-heating test methodology. The aerogel blanket was of a 20 mm thickness and implemented with a 12 mm of gypsum plasterboard. The pre-retrofit heat loss coefficient was 17.15 W/K and after the installation of the aerogel blanket, the heat loss was recorded as 6.29 W/K. This is a reduction of 63%.

In silica aerogels, radiation and solid conduction are significant modes of heat transfer. Reducing density will decrease solid conductivity because of a reduction in contact area between the particles. However, this reduces optical density which increases infrared radiation. In silica aerogels, infrared radiation between 3-8 μm has a low absorption coefficient. Silica aerogels doped with carbon can drastically reduce heat transfer through radiation because of carbon's high absorption coefficient. Zeng et al. [45] proceeded to find the optimum amount of carbon to minimize heat transfer. This was done theoretically by using energy equations for coupled conduction and radiation. It was found that 8% of carbon content in silica aerogels reduced heat transfer by about 1/3 at ambient temperatures.

Lu et al. [46] measured thermal conductivity in carbon aerogels using a transient hot-wire technique. It was shown that in carbon aerogels, solid thermal conductivity was much higher as it is directly proportional to density. They found that the thermal conductivity was 0.029 W/mK at ambient air temperatures. The radiation component

was found to be negligible because of a high specific extinction coefficient. Comparing it to thermal conductivity measurements taken in the evacuated state, gaseous conductivity was found to be between 0.005 W/mK and 0.011 W/mK. However, compared to silica and organic aerogels, the thermal conductivity is higher because of relatively larger pore sizes.

Chapter 3
Characterization of test specimens

Two test specimens were used in the experiments, they were Cabot's Thermal Wrap (Fig. 6 (a)) and Aspen's Spaceloft (Fig. 6 (b)). They were both flexible blankets of a thickness between 5 to 6 mm. Characterization was carried out on both blankets to compare and analyze differences in their structure and composition.

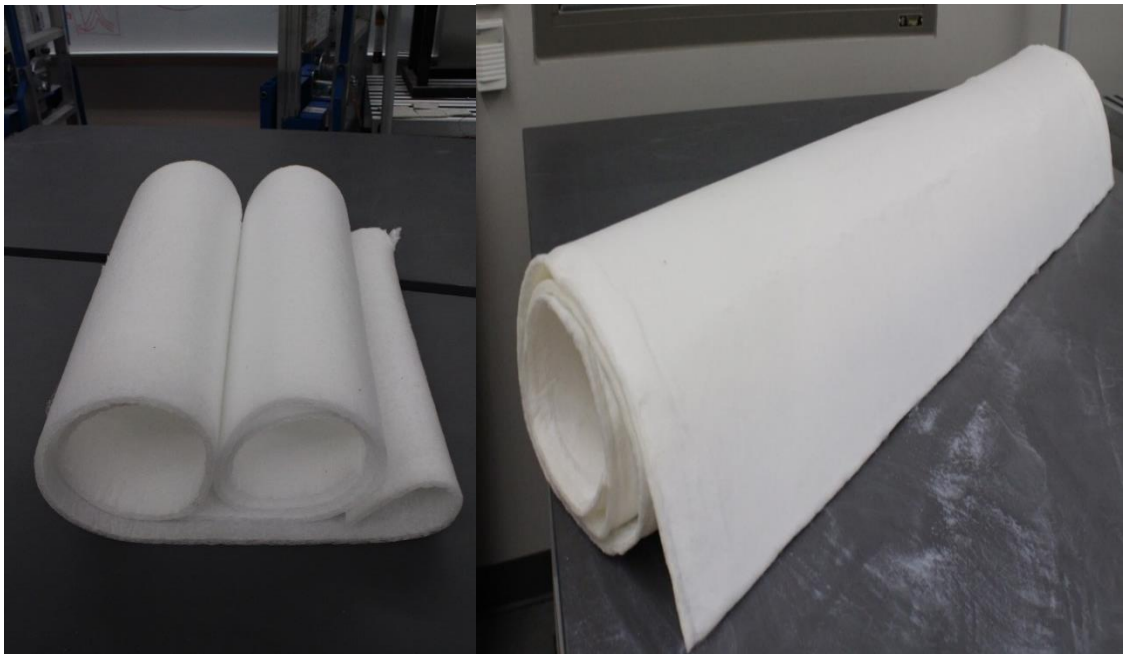

(a) **(b)**

Fig. 6. Aerogel blankets
(a) Cabot's Thermal Wrap and (b) Aspen's Spaceloft blanket.

Cabot's Thermal Wrap was sealed in plastic sheets and arrived in rolls of size 0.56 m x 1.21 m. Aspen's Spaceloft arrived unsealed in a large roll of width 1.45 m. The length can be specified while ordering.

3.1. Electron microscopy

Aerogels have a unique nanostructure consisting of a number of interconnected silica filaments which border nano sized pores. At filament junctions a number of filament connect to form a web like structure. The solid portion of aerogel is less than 1%. This results in a number of aerogels properties, including its low thermal conductivity. The nano-structure of aerogels in the blankets was examined using an FEI Versa 3D Dual Beam electron microscope (Fig. 7), which is a scanning electron microscope.

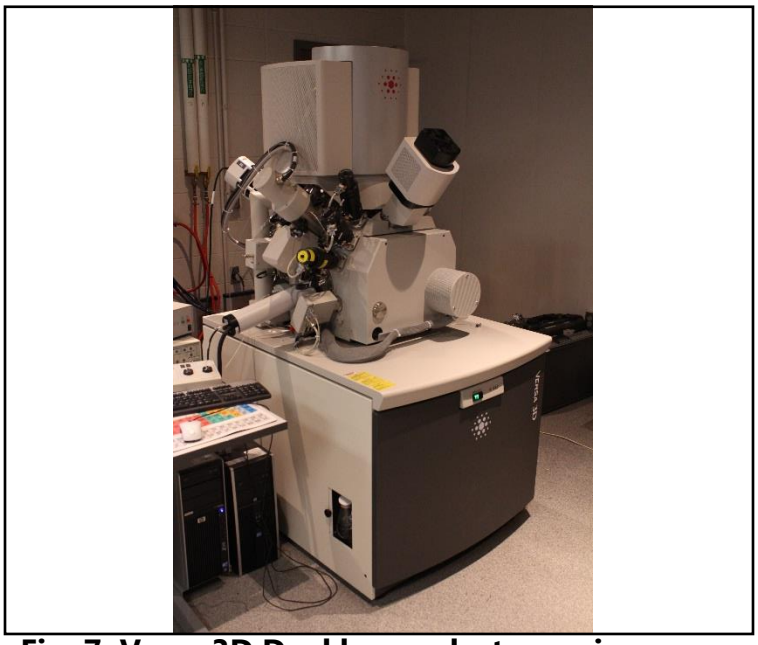

Fig. 7. Versa 3D Dual beam electron microscope.

An electron microscope uses a high voltage gun that shoots accelerated electrons onto a specimen. These microscopes allow more detail and a larger magnification than a light microscope because of the smaller wavelengths of electrons as compared with light,

which allows it to interact with the specimen at a smaller scale. After the electrons interact with the specimen it ejects secondary electrons that are detected to form the image. For all imagining purposes Everhart-Thornley SE detector (ETD) and In-column Detector (ICD) were used. Often because of the non-conductive nature of the specimen, imaging becomes more of a challenge. In Fig. 8 the aerogel sample was coated with gold nano-particles to allow it to be imaged clearly and to give the pore structure a depth dimension. Both aerogel samples showed a similar nanostructure.

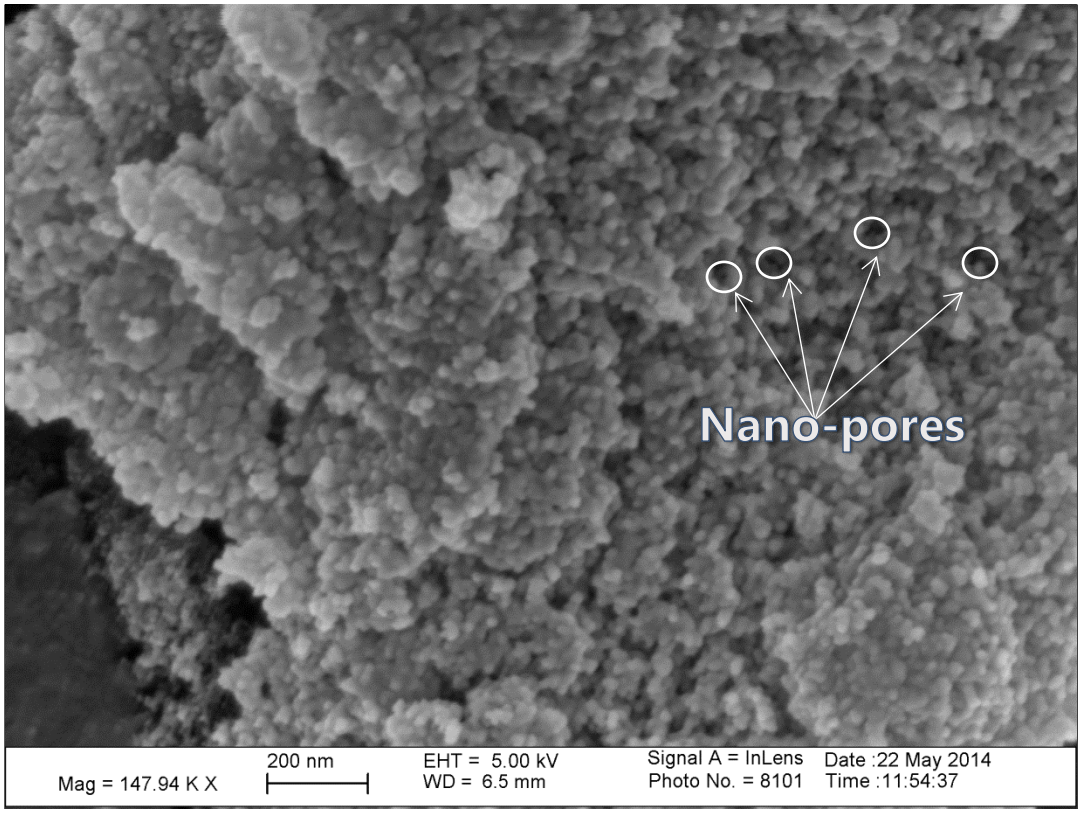

Fig. 8. Pore structure.

Pore sizes ranged from 10 nm to 200 nm (shown in black). These smaller pore sizes work to reduce thermal conductivity through aerogels as was explained in section 1.2.3. To get a more accurate estimate of pore sizes and internal surface area, a

Brunauer–Emmett–Teller (BET) test can be conducted. BET theory works by measuring the physical adsorption of a gas by the surface. Some typical values for surface area are between 100-1000 m^2/g. Further, energy-dispersive X-ray spectroscopy was used to identify the primary elements in aerogel.

3.1.1. Cabot's thermal wrap

The properties of the thermal wrap are listed in Table 5. The thermal wrap also had sound insulation properties. The thermal wrap was a white flexible blanket, with polyester and polyethylene fibers placed in layers parallel to the plane of application. Inside the blanket was a random embedment of aerogel dust (in blue) that is shown in Fig. 9. In Fig. 9, some of the dust was colored using editing software to show contrast in the SEM image. The approximate volumetric percentage of aerogel was calculated. First, three samples of size 5 cm x 5 cm were prepared. The aerogel dust present inside the blanket sample was weighed and compared with the weight of the blanket. To find its volume, the weight of the aerogel dust and the blanket were divided by their respective densities. By volume, there was about 33% of aerogel in these blankets.

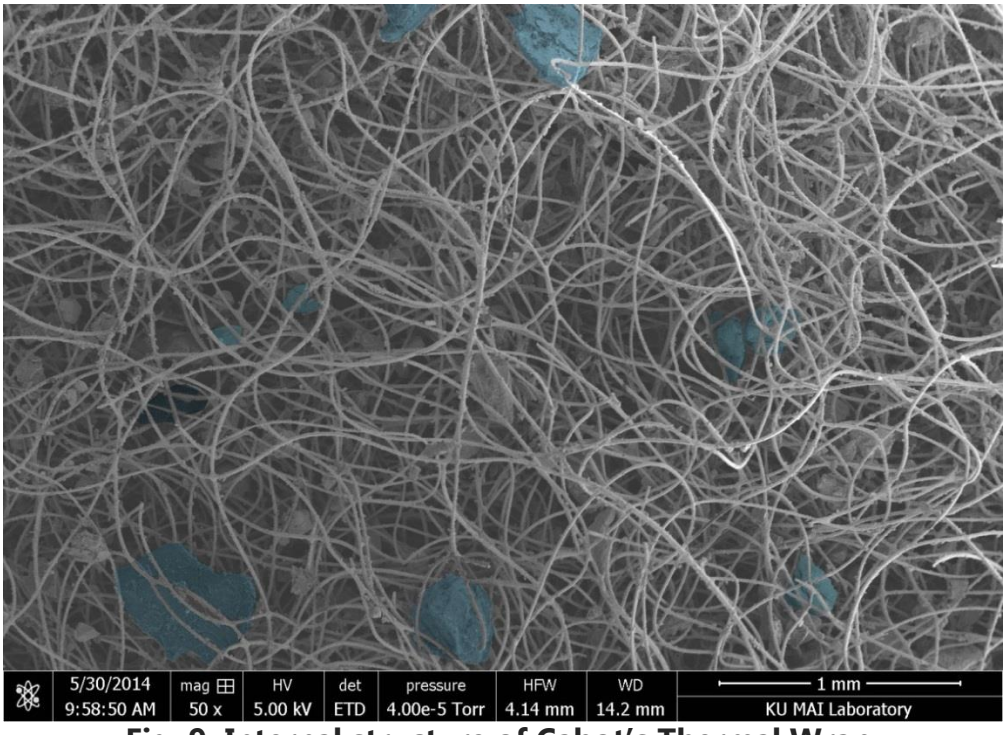

Fig. 9. Internal structure of Cabot's Thermal Wrap.

In the blanket there were two heat resisting systems. The fibers that work to trap air at a macro level and the aerogel dust that works at the nano scale range. The blankets were not sealed at its edges causing aerogel dust particles to fall out while handling. This may affect the performance of the blanket.

Table 5
Properties of Cabot's Thermal Wrap [47].

Property	**Value**
Thickness	6 mm
Density	~70 kg/m^3
Fiber composition	Polyester and polyethylene
Tensile strength	517 kPa
Operating temperature	-200 to 150 °C continuous (160 °C peaks)
Light transmission	~20% at 8 mm

The operating temperature range was from -200 to 150 °C. However, according to the manufacturer, the aerogel blanket does not perform consistently throughout this range because it shows a higher thermal resistance at lower temperatures [48]. The 6 mm thermal wrap was selected for testing because of its unusually low thickness which allows flexibility of application.

Energy-dispersive X-ray spectroscopy (EDX) was used to determine the composition of the aerogel dust (Fig. 10). EDX works on the basis that every element has a different atomic structure and on excitation emits unique x-ray patterns that are used to characterize the element [13]. This allowed for the material and quantitative analyses of the aerogel. The aerogel was found to be dominantly silicon and oxygen which implied that it was silica based.

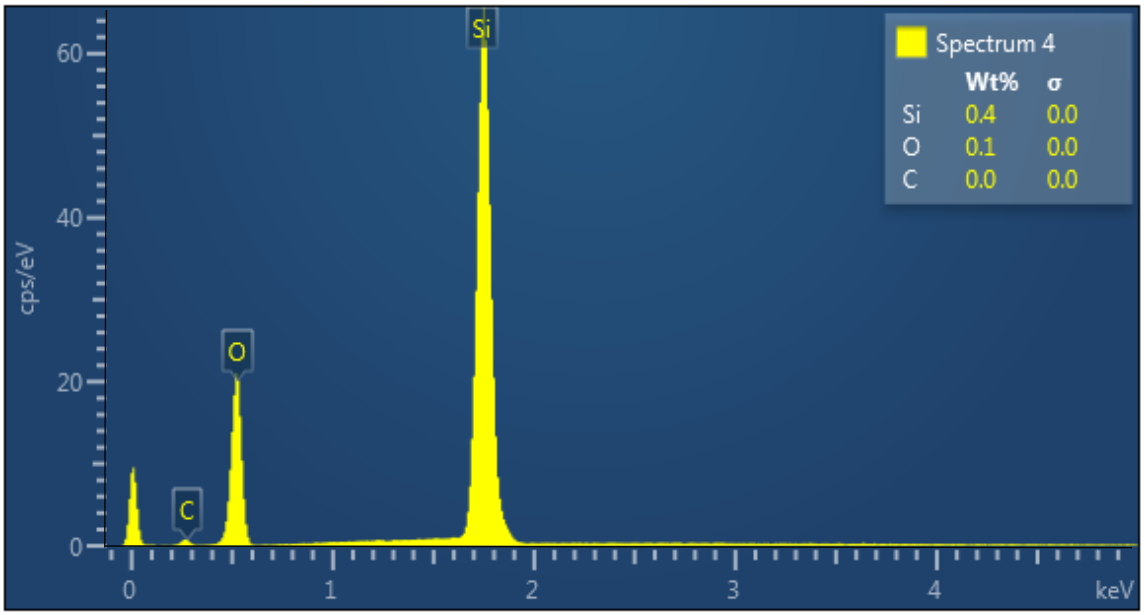

Fig. 10. Graph showing the composition of aerogel in Cabot's Thermal Wrap.

The ordinate axis indicated counts per second per electron volt (cps/eV). This is a measure of the intensity of the x-rays emitted. The abscissa represented the energy levels of the x-rays in kilo electron volt.

3.1.2. Aspen's Spaceloft blanket

The properties of Aspen's Spaceloft blanket are listed in Table 6. This blanket was also white and was coated on both the inside and outside with aerogel dust. Fibers were made of polyethylene and fibrous glass. The picture shown in Fig. 11 was taken at the same magnification (50X) as that of Cabot's Thermal wrap (Fig. 9).

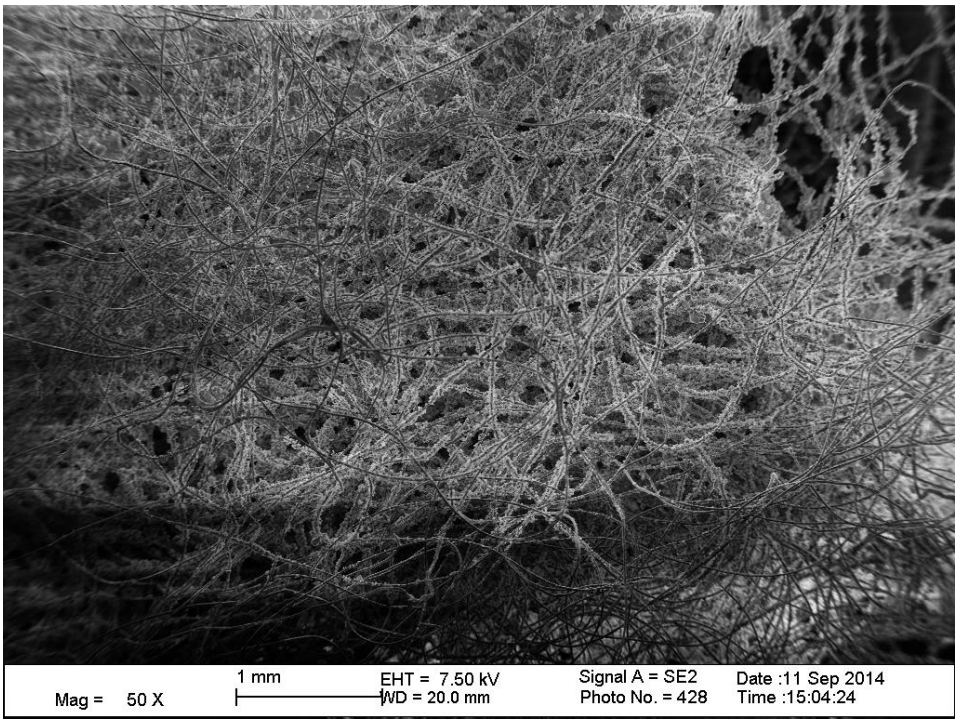

Fig. 11. Internal structure of Aspen's Spaceloft.

Aspens Spaceloft used a fiber size of a smaller diameter that allowed it to be packed more densely. The density of Aspen's Spaceloft was approximately twice that of Cabot's Thermal wrap. A more detailed picture of the fiber strands is shown in Fig. 12.

Table 6
Properties of Aspen's Spaceloft [46].

Property	Value
Thickness	5 mm
Density	150 kg/m^3
Fiber composition	Polyethylene and fiberglass
Hydrophobic	Yes
Operating temperature	200 °C (maximum)
Light transmission	Yes

The main difference in the aerogel which was used was the size of the crystals. Aspen's Spaceloft had aerogel dust that was smaller and more uniform in size. These aerogel particles were more likely to attach themselves to the fibers (Fig. 12). The approximate average size of the particles in Aspen's Spaceloft blanket was a quarter of those in Cabot's Thermal Wrap.

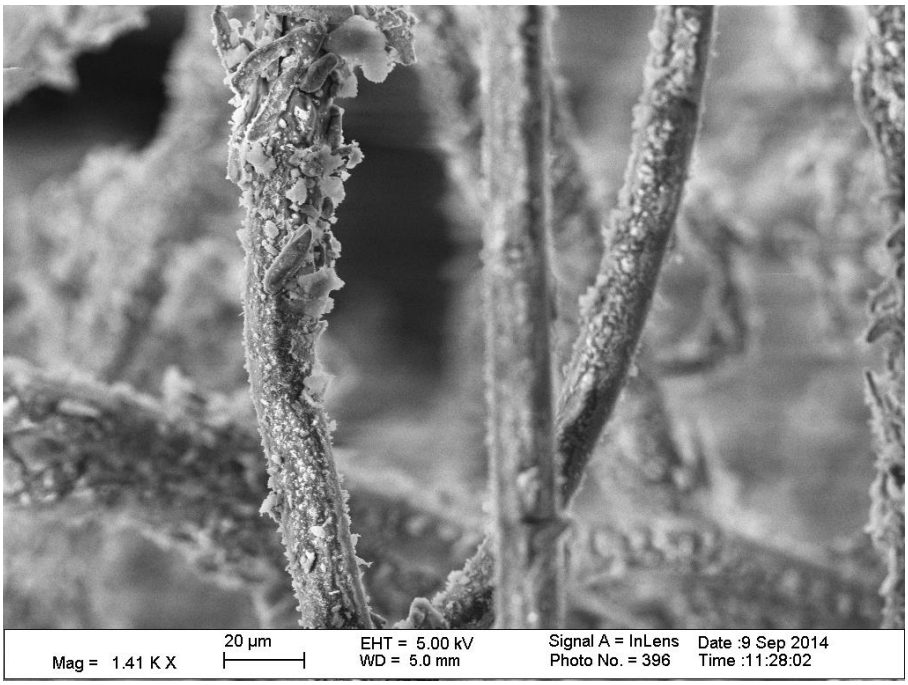

Fig. 12. Fibers in Aspen's Spaceloft.

The approximate volumetric percentage of aerogel was calculated in the same way as was done previously for Cabot's Thermal Wrap. First, three samples of size 5 cm X 5 cm were prepared. The dust present inside the blanket sample had about 10% calcium silicate and 5% synthetic graphite by volume [49]. The volumes of these materials were calculated based on the sample size and multiplied by their densities to get the weight of the respective compounds. It was found that there was 42% aerogel dust by volume. This is 9% more aerogel dust than was found in Cabot's Thermal Wrap.

EDX was conducted on the sample to check if there were any other significant elements in the aerogel dust. The EDX confirmed the presence of silicon and oxygen (Fig. 13). The SEM was focused on an aerogel dust crystal at the time of measurement.

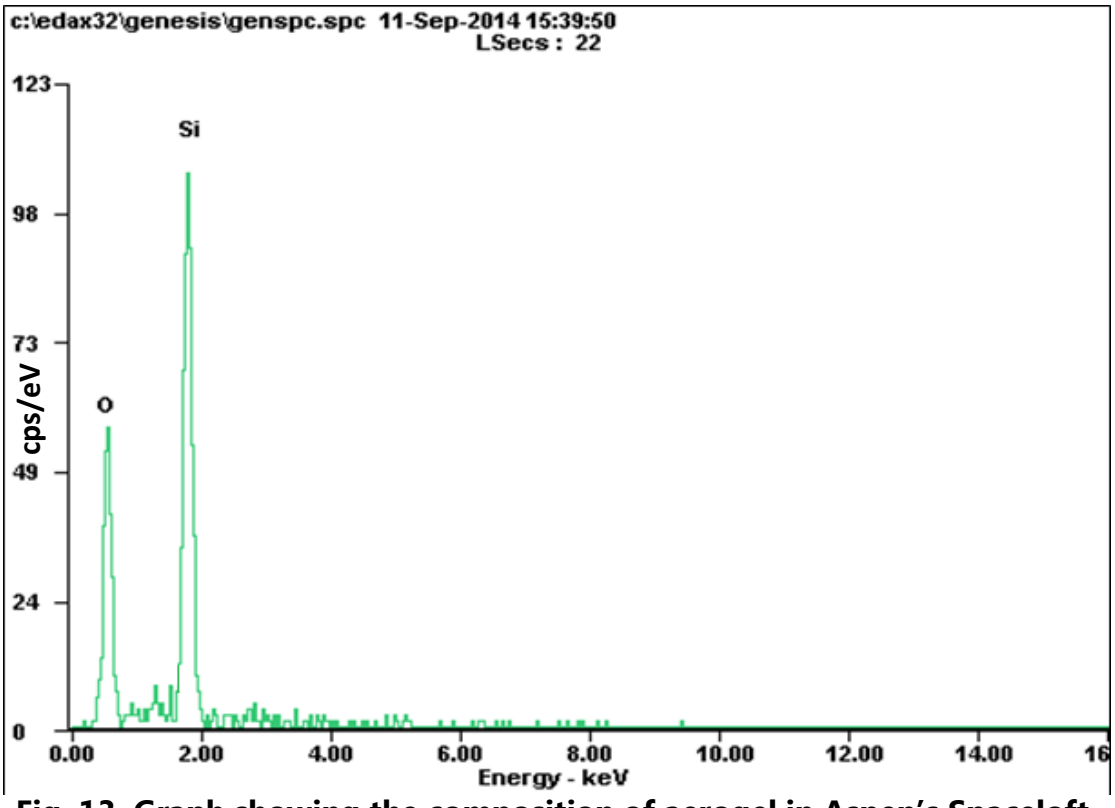

Fig. 13. Graph showing the composition of aerogel in Aspen's Spaceloft.

Chapter 4
Experimental setup

4.1. Measurement, Materials, and Sustainable Environment Center (M2SEC) Building

This building is located on the campus of the University of Kansas. Partial funding for the building was provided by the National Institute of Standards and Technology (NIST). It is a building that is exclusively for research and was built with this in mind. The buildings enclosure can be used to collect heat and mass transfer data across its components. Shown in Fig. 14 are the south and west walls of the M2SEC building.

Fig. 14. M2SEC building.

There are a total of 60 interchangeable panels, of which 30 are in the south wall and 30 are in the west wall. These interchangeable panels allow different building materials to be tested. For this research three panels were selected in the south wall on the ground floor as indicated in Fig. 15.

Fig. 15. Instrumented panels.

Inside the building, there is an easement provided on the ground and first floor of the building which allows the panels to be retrofitted and instrumented. The easement is shown in Fig. 16. Access to the easement is restricted to prevent disturbances to the data collected. Above the easement is a metallic tray extending along the length of the corridor. This can be used to hold instruments and wiring.

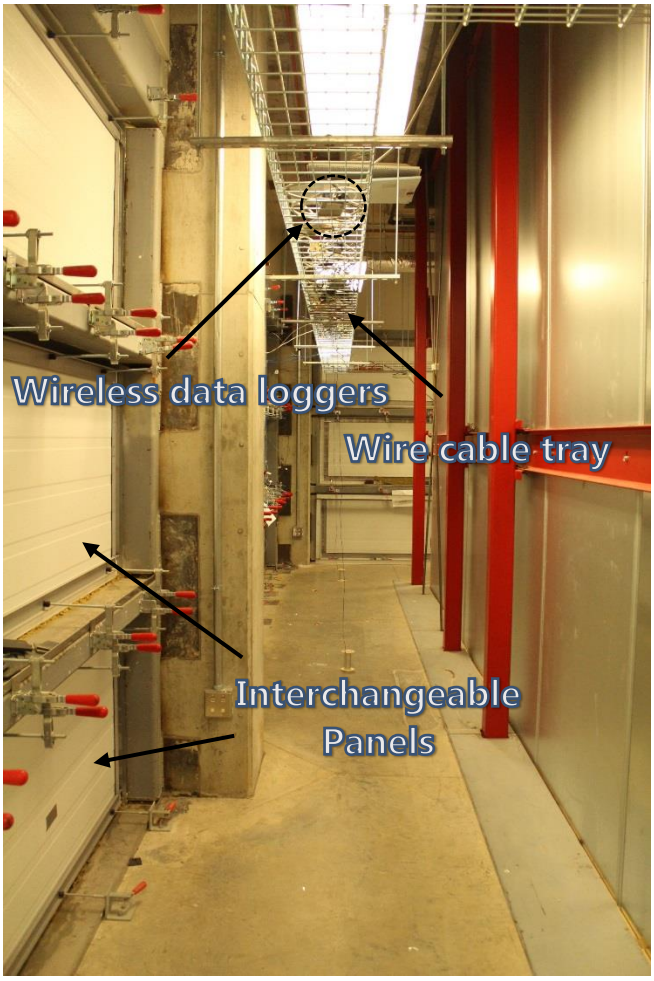

Fig. 16. M2SEC easement.

The panels are shown in greater detail in a photo taken from inside the M2SEC building (Fig. 17). In the picture of Fig. 17, the panels are unclamped and in an open position. The original panels comprise of a foamed insulation at its core, a metallic-coated steel sheet at its exterior, and a siliconized polyester as an interior finish. Each panel had a size of 1.62 m x 0.88 m, a thickness of 76 mm, and a nominal minimum total thermal resistance of 2.82 m^2K/W. These panels can be fastened by the use of self-tapping screws with rubber tips that act as clamps. These fasteners can be adjusted to fit panels of different thicknesses. The contact point between the rubber tips and the

interchangeable panel is a metallic frame. The metallic frame is cold rolled and acts a stiffer contact point between the fastener and the panel.

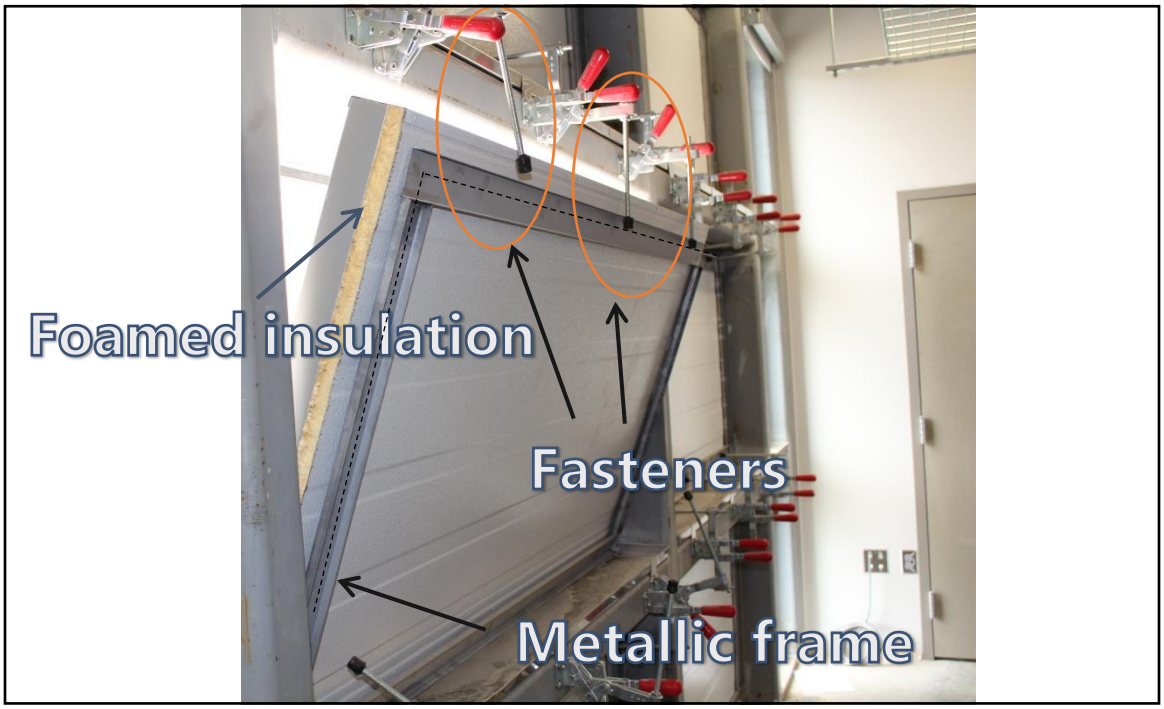

Fig. 17. Interchangeable panels.

4.1.1 Space cooling system

The interior of the M2SEC building was air conditioned by a central air conditioning system. The thermostat for the easement was set to 23.3 °C. There are five air handling units (AHU's) that were used to control air flow through the building. There was no recycling of air and all the air was 100% exhausted. The main chiller unit was a 1072 kW air-cooled unit which was used in conjugation with smaller modular units. These operated in a glycol water loop to chill the building. Additionally, chilled water

pipes are exposed (chilled beam technology) in most areas of the building which reduces the load on the AHU's.

4.2. Data acquisition system

A National Instruments NI-Cdaq-9191 (Fig. 18) wireless unit was used. This chassis can be fitted with a number of modules to suit the required measurements. For this research, module NI 9213 was used which was a 16-channel thermocouple and millivolt input module, which was also used to acquire heat flux data.

Fig. 18. Data logger with measurement module.

These wireless units work by transferring data through local area wireless technology (Wi-Fi). This can be done by using a carrier signal that is generated by other devices or it can generate its own signal which can be used to form an ad hoc network with a host computer. Also, it has the ability to acquire data via Ethernet cable. Typically, the range of the wireless system is 30 m in an indoor environment. However, in the presence of thicker walls, this range drops drastically and the use of the Ethernet cable becomes necessary. Being wireless, it provides flexibility in its use and the elimination of an untidy wired system. The wire cable trays shown in Fig. 16 were used to house the data loggers on the ground floor of the building. The host computer was on the first floor and data were transferred using NI's signal express data acquisition software. However, the initial setup was done through NI MAX, which is a software provided by National Instruments to facilitate connectivity with the host computer.

4.3. Wall panel setup

The three panels selected in the south wall were fitted with cement boards while maintaining an air gap of six millimeters between the panel surface and the cement board using spacers. The board and panel were fitted with the required instrumentation, namely, thermocouples (T/C) and heat flux meters (HFM) and calibrated to make sure that temperatures and heat fluxes matched evenly between all three panels (Fig. 19). There were a total of two heat flux measurements and four temperature measurements that were collected for each panel. The four temperature measurements were for the exterior panel surface, the air space panel surface, the air space cement board surface,

and the interior cement board surface. Two heat flux meters were attached to the interior cement board surface.

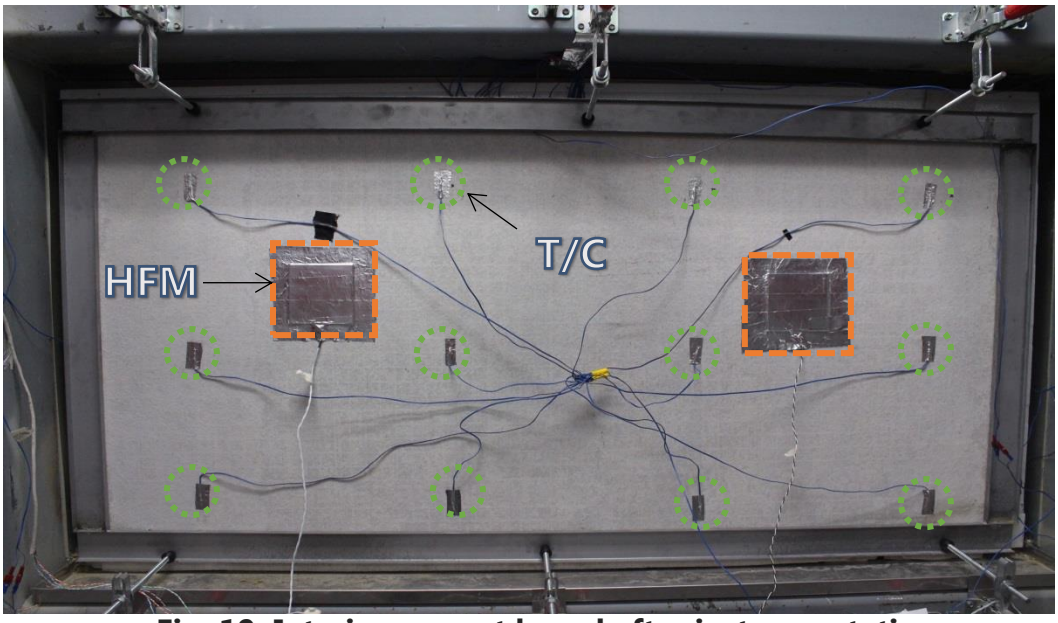

Fig. 19. Interior cement board after instrumentation.

The second set of data collected was for the retrofit. The panels were fitted with the aerogel blankets and a polyester insulation board between the cement board and the panel surface (Fig. 20). The panel in the center was left with an air gap between the cement board and the panel surface to serve as the control for the experiments.

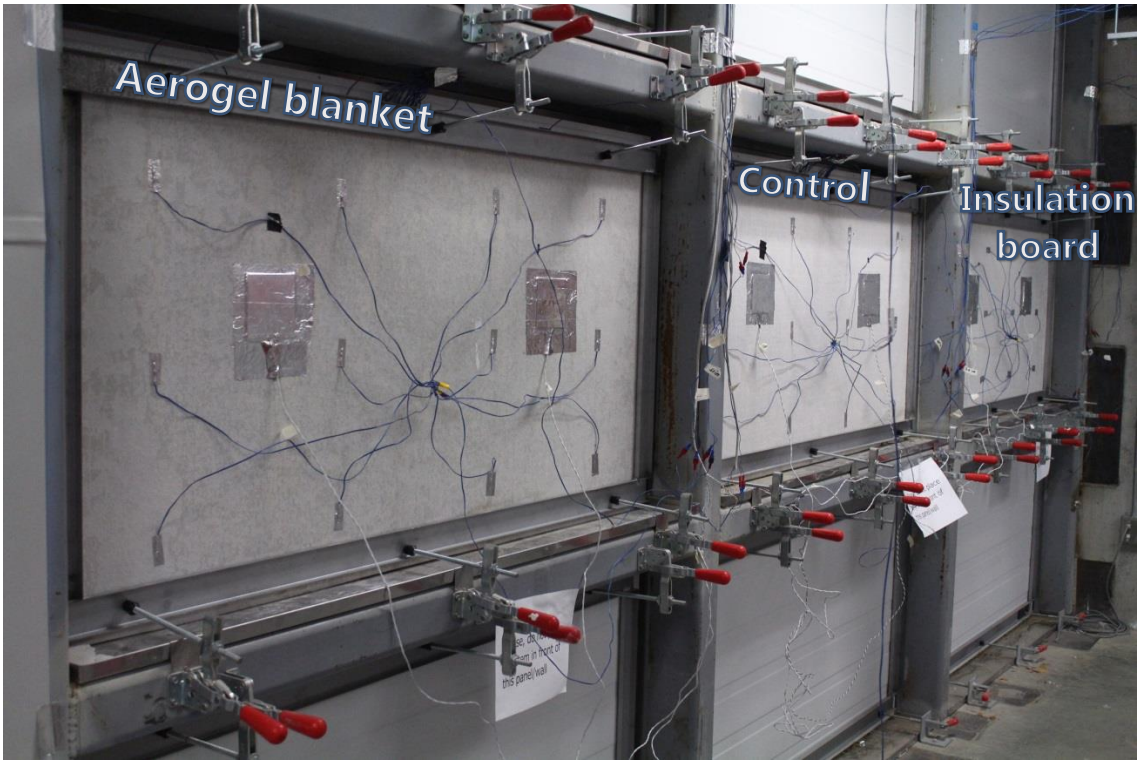

Fig. 20. Tested panels.

4.4. Temperature measurements

For temperature measurements, type T thermocouples were used. This is a thermocouple type that is made from copper and copper-nickel wires and can be used for a wide range of temperatures. For each surface 12 thermocouples were attached in parallel to form a grid that measured average surface temperatures. The T/Cs were attached using aluminum tape to reduce gain and loss of heat through radiation effects. According to the manufacturer, T/Cs may show an error of ±0.5°C.

In each panel, for the four layer surfaces (i.e., exterior panel surface, air space panel surface, air space cement board surface, and interior cement board surface), a total of 48 T/Cs, were attached. Thermocouples were also used to measure ambient air

temperatures. Two for the indoor air temperature (Fig. 21 (a)) and two for the outdoor air temperature (Fig. 21 (b)).

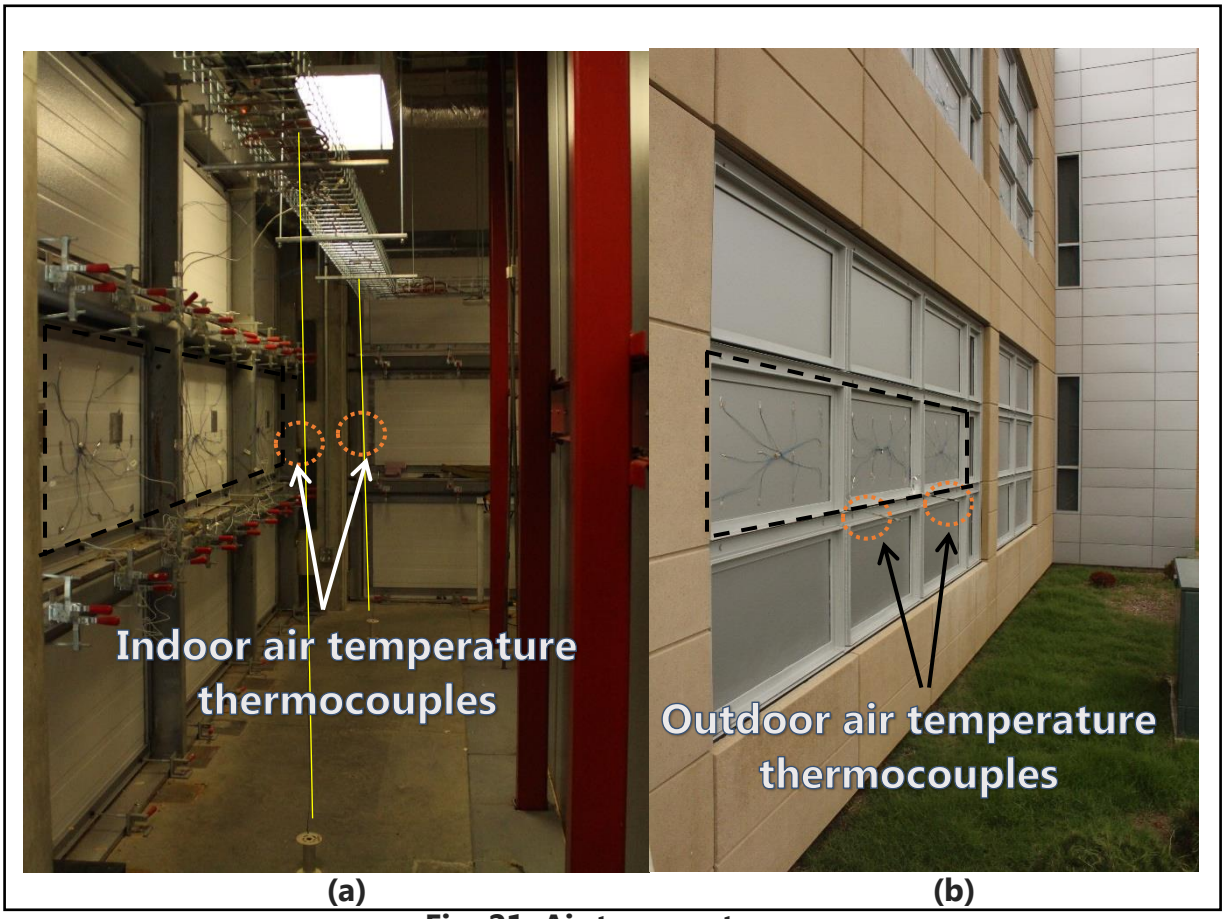

Fig. 21. Air temperatures
(a) indoor air temperature and (b) outdoor air temperature.

The thermocouples used to measure ambient air temperature were also wrapped in aluminum tape to reduce radiation effects. The outdoor and indoor air temperature T/Cs were kept away from the surface of the panels to reduce interference from the thermal radiation re-radiating from the surface of the panels.

A schematic diagram is used to show the placement of the T/Cs on the panel (Fig. 22). The location of the T/Cs are marked by 12 green circles.

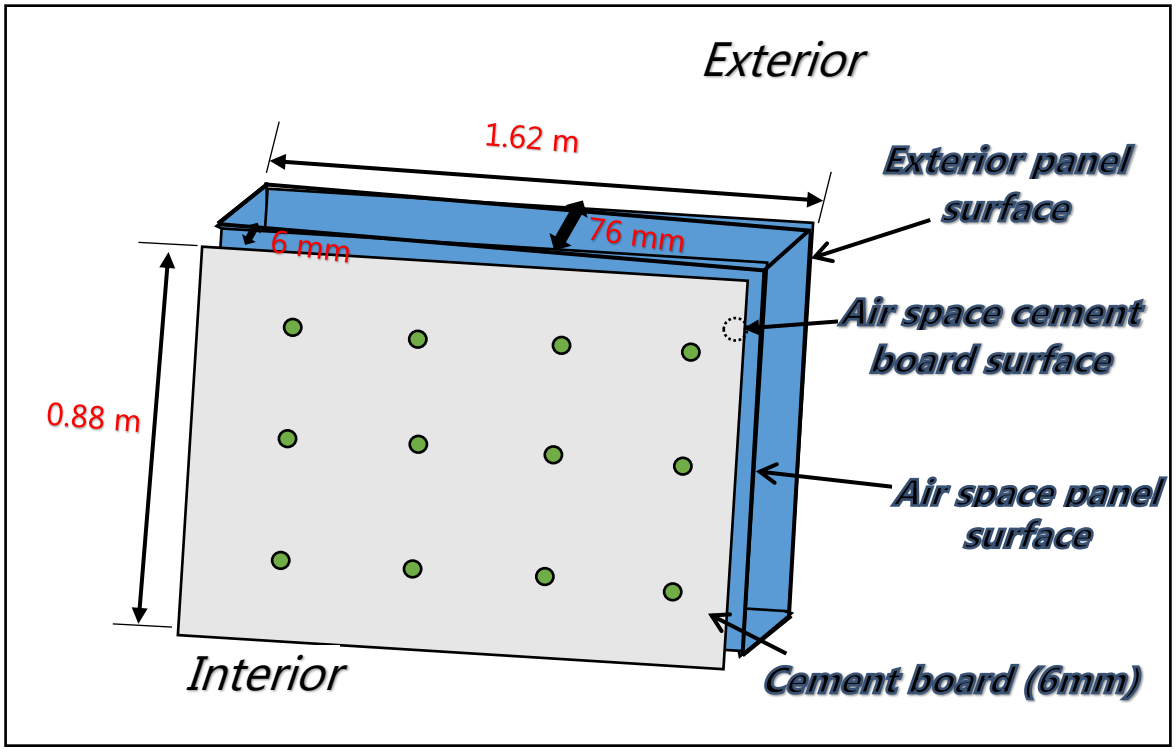

Fig. 22. Thermocouple placement.

4.5. Heat flux measurements

Heat flux measurements were made using a total of six heat flux meters, two for each panel. Each heat flux meter was 10.16 cm x 10.16 cm x 0.27 cm. They were attached to the cement board surface using aluminum tape. For each panel heat fluxes were averaged between the two heat flux meters. A schematic diagram is used to show the placement of heat flux meters on the panel (Fig. 23). The location of the HFMs are marked by two orange squares.

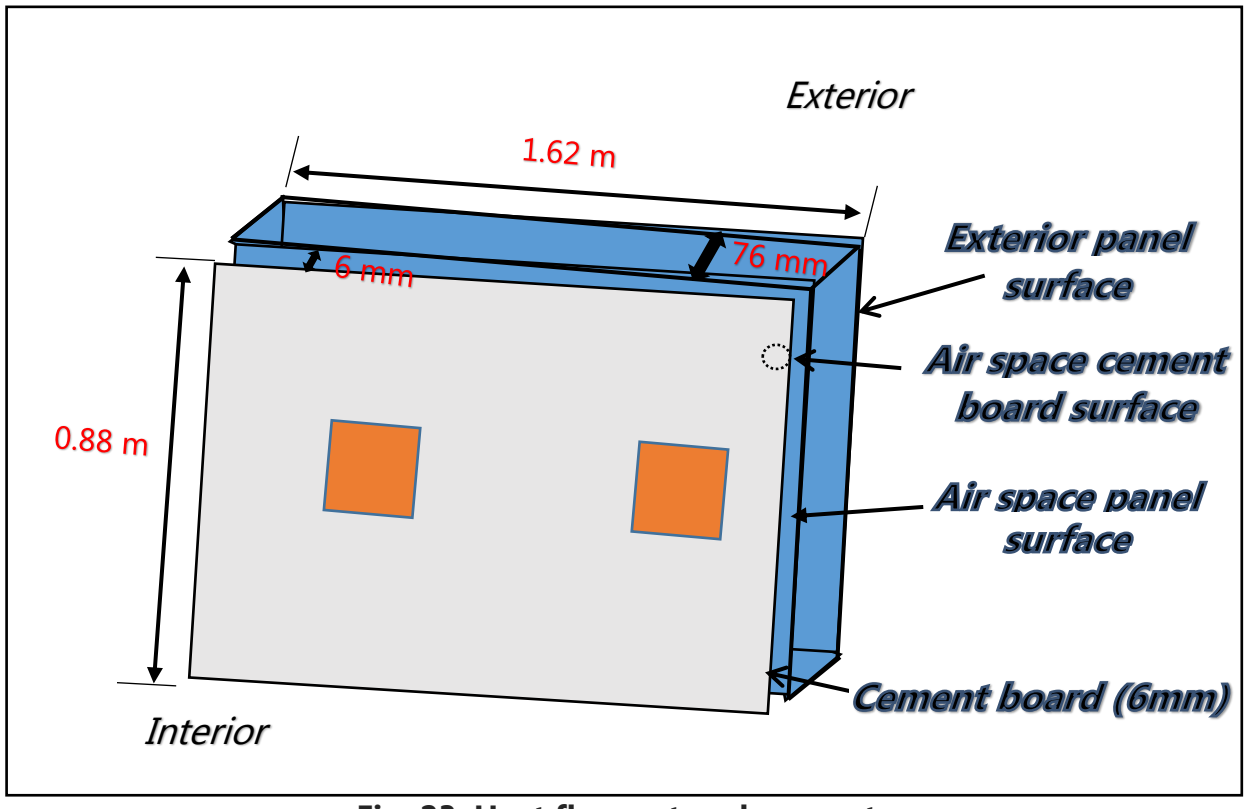

Fig. 23. Heat flux meter placement.

Chapter 5
Experimental results and discussion

Two sets of data were collected using three panels. The first set was for the pre-retrofit and the second was for the retrofit. In both cases heat flux and temperature data were collected. The experiments were conducted over the duration of the summer (May, June, July, and August) for the panels located in the south wall.

5.1. Pre-retrofit thermal performance

Sometimes because of the shape, orientation and fenestrations of a building, thermal performance may vary in different sections. During the pre-retrofit phase calibration tests were conducted to confirm an equal thermal performance between the three panels. The panels are labelled in Fig. 24.

Fig. 24. Labeled panels.

5.1.1. Surface temperatures

Surface temperatures were measured at four different layers that made up the panel assembly. The average exterior surface temperature for panel 1 was 26.30 °C for the calibration period. Panel 2 had an average surface temperature of 26.28 °C and panel 3 had an average surface temperature of 26.33 °C. Panel 2 was selected as the control panel, and therefore, the temperature differences between panel 1 and panel 3 in relation to panel 2 were -0.02 and +0.03 °C, respectively. The average interior surface temperatures were 22.0 °C, 22.20 °C, and 22.36 °C for panel 1, panel 2, and panel 3, respectively. When compared to panel 2, panel 1 showed a difference of -0.2 °C and panel 3 showed a difference of +0.16 °C. That is the difference in surface temperatures for the exterior and interior surfaces were less than 0.03 and 0.2 °C, respectively. Considering the changes in amplitude that occur for exterior surface temperatures (Fig. 25), this exhibits the careful instrumentation and control that was carried out to get this level of accuracy.

The air space formed in between the cement board and the panel surface (Fig. 23) was instrumented with T/Cs. Care was taken so that the T/Cs did not touch and were adhered to the surface properly because they could not be visually inspected until the cement board was removed. The average air space panel surface temperatures were 22.0 °C, 22.18 °C and 22.30 °C. The temperature differences when compared to the control (panel 2) were +0.18 °C and -0.12 °C for panels 1 and 3, respectively. The average air space cement board surface temperatures were 21.63 °C, 21.87 °C, and 22.01 °C. This represented a temperature difference of 0.24 °C (panel 1) and 0.14 °C (panel 3) in relation to panel 2, respectively.

Heat transfer can occur at increased rates when the air surrounding the panels is being replaced by air at a lower or higher temperature and/or the motion of the air is increased. Inside buildings this may be caused by the flow of air from an air-conditioning outlet duct. Outside the building, wind eddies often create separated flow zones around sharp edged buildings [50]. Measurements for the indoor air and outdoor air temperature were taken to check for consistency. Fig. 25 shows conformity between the two outdoor air temperature measurements shown in Fig. 21 (b). Fig. 26 is for the indoor air temperature measurements, which correspond to the probes shown in Fig. 21 (a).

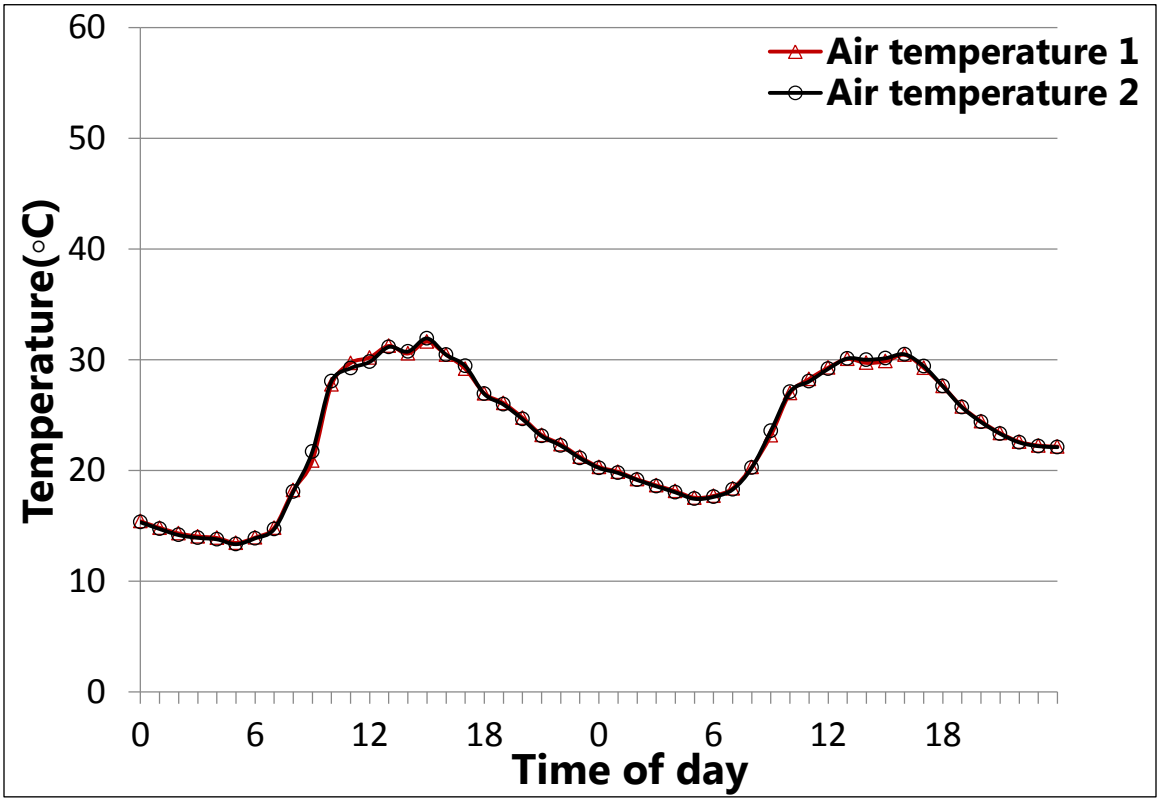

Fig. 25. Outdoor air temperature comparison during pre-retrofit test.

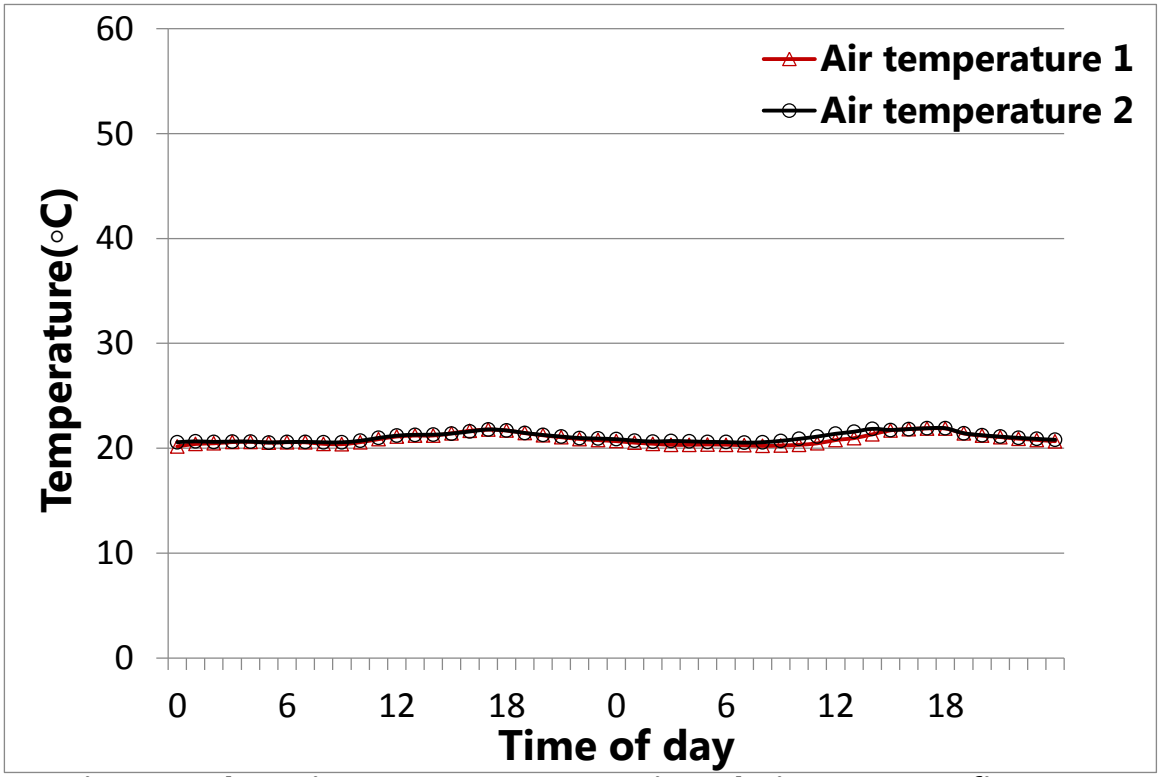

Fig. 26. Indoor air temperature comparison during pre-retrofit test.

The surface temperatures are summarized in Table 7.

Table 7
Summary of average surface temperatures during pre-retrofit test.

Average temperatures	Panel 1 (°C)	Difference in relation to panel 2	Panel 2 (°C) Control	Difference in relation to panel 2	Panel 3 (°C)
Exterior surface	26.30	0.02	26.28	0.04	26.33
Air space panel surface	22.00	-0.21	22.20	0.15	22.36
Air space cement board surface	22.01	-0.16	22.18	0.12	22.30
Interior cement board surface	21.63	-0.24	21.87	0.14	22.01

It can be noted that the data in Table 7 show that the temperature differences were less than +/-0.25 °C. This showed how closely the data was matched. Surface

temperature readings also showed a clear difference in temperatures between the exterior and interior surfaces which induced heat transfer towards the interior of the building. Fig. 27, 28, 29, and 30 show the trend of exterior panel surface, air space panel surface, air space cement board surface, and interior cement board surface temperatures, respectively.

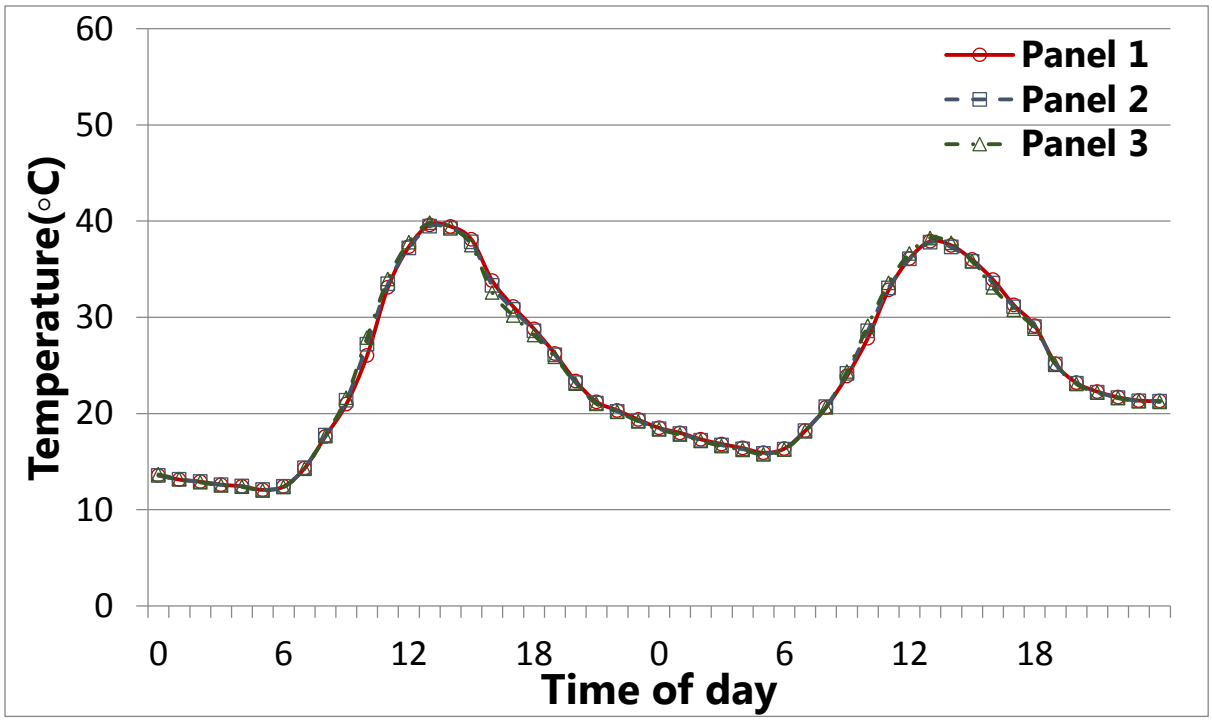

Fig. 27. Exterior surface temperatures during pre-retrofit test.

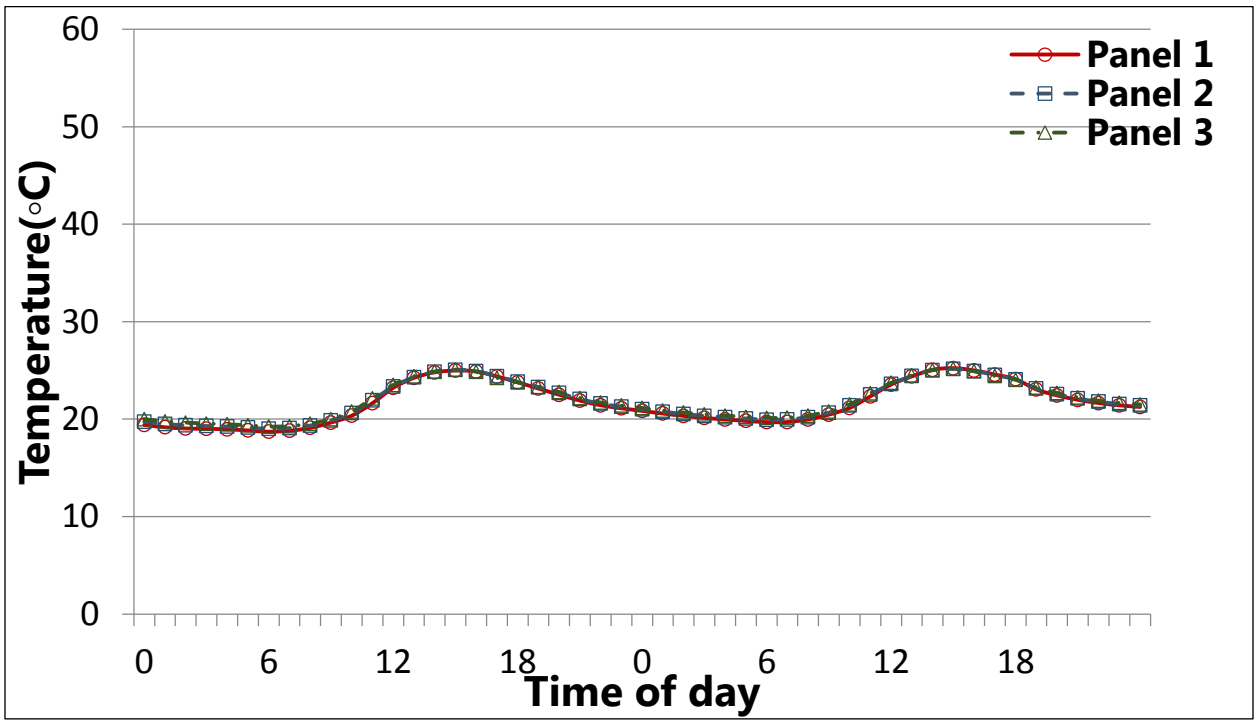

Fig. 28. Air space panel surface temperatures during pre-retrofit test.

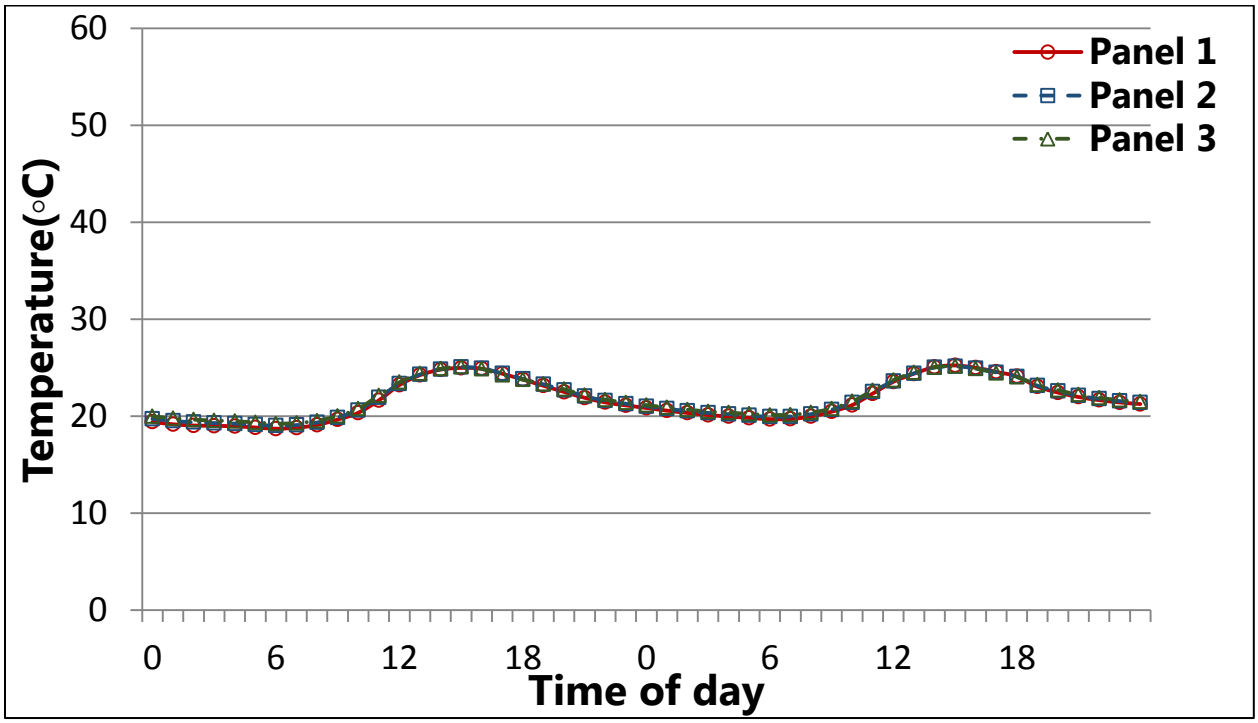

Fig. 29. Air space cement board surface temperatures during pre-retrofit test.

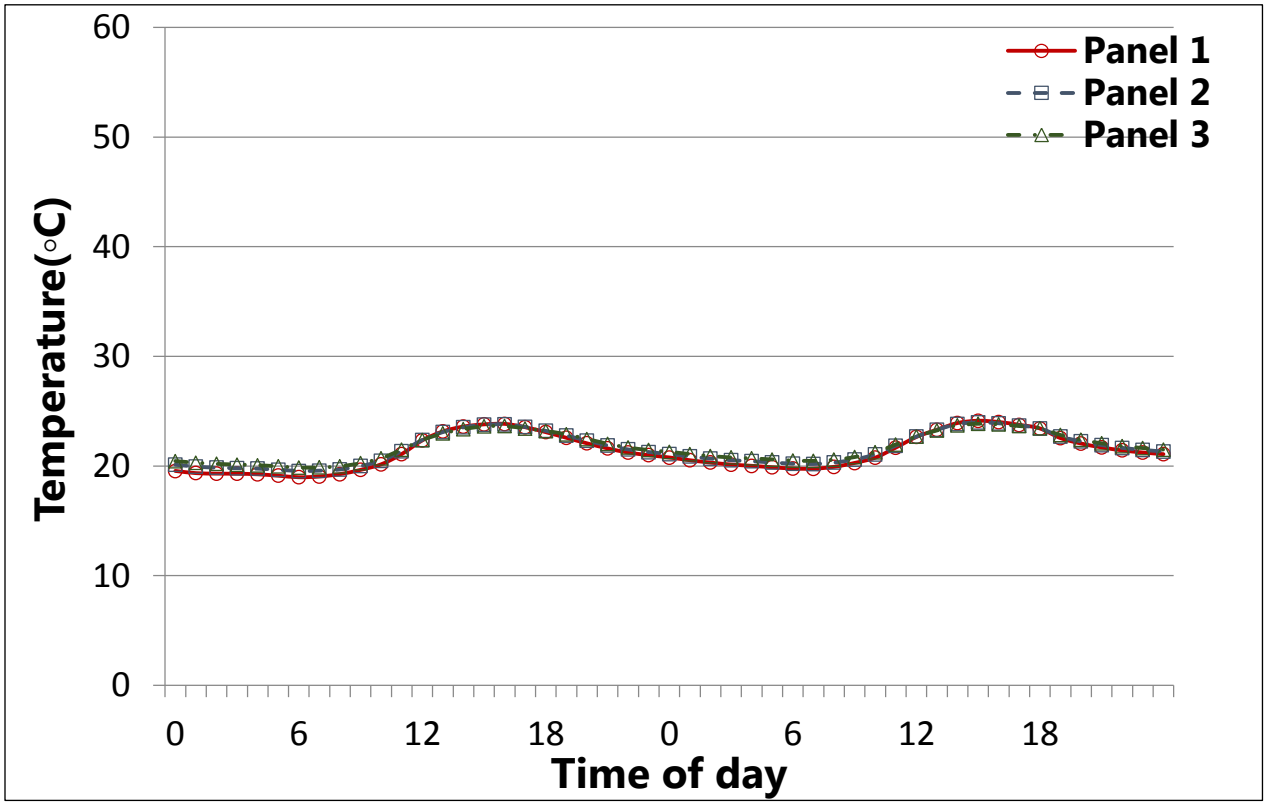

Fig. 30. Interior surface temperatures during pre-retrofit test.

Outdoor temperatures and weather conditions are constantly changing; therefore, this prevents steady state heat flow, which makes temperatures more prone to fluctuations. Data were collected every 10 seconds and averaged hourly from the 12 T/Cs placed on each layer surface. This allowed data collected to reach a fair level of accuracy. It can be concluded that the thermal behavior of the three panels was similar.

5.1.2. Heat fluxes

The data shown is for a 48 hour period during the calibration phase (Fig. 31). The difference in heat flux at the peaks when compared to the control was 4.9% for panel 1 and 3.5% for panel 3.

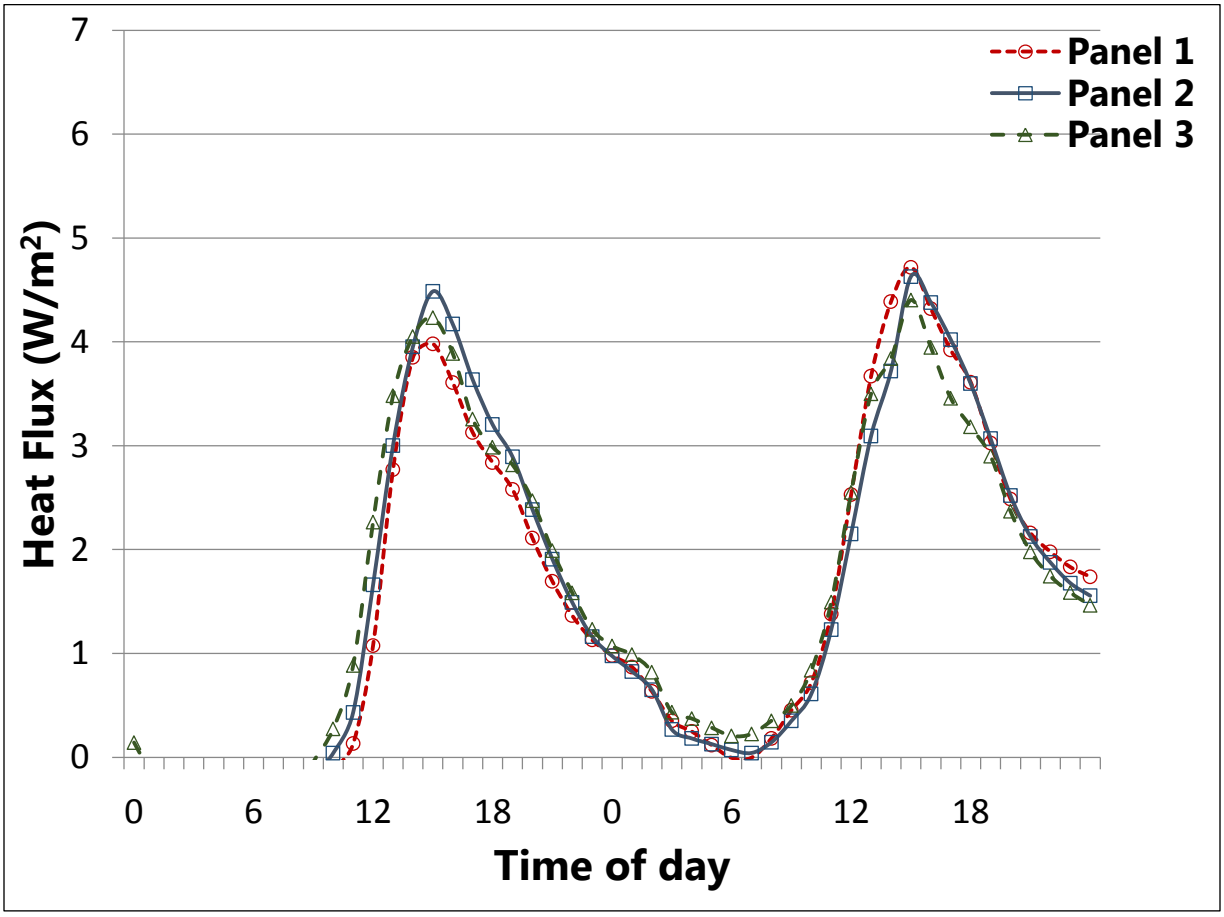

Fig. 31. Heat fluxes through panels during pre-retrofit test.

This difference is acceptable when considering that heat flux meters are not as accurate as temperature sensors. To understand this it is necessary to examine how a heat flux meter works. A heat flux meter is a solid state transducer comprised of two surfaces, one of which is in contact with the surface through which the heat flux is to be measured. On

the inside, both the surfaces are in contact with a thermopile, which is essentially a number of thermocouples in series. This thermopile is embedded in an insulating matrix and converts the temperature differential into a voltage that is read by the data logger. This is a highly sensitive setup that may be affected from sudden changes in temperature, air flow, and humidity. Moreover, view angle, wavelength, and dominant mode of heat transfer play an important role [51]. To address this issue heat flux meters were recalibrated before application to make sure that their k-values were accurate.

Another source of heat flux error is the fact that surfaces are not completely even and do not form a contact at all points on its surfaces. This is because no surface is completely flat and at a microscopic level do have variations. Care was taken, however, to maximize contact and prevent any unevenness while attaching the heat flux meters by removing dust, cleaning both surfaces, and attaching the heat flux meters firmly.

5.2. Retrofit thermal performance

The two blankets tested were Cabot's Thermal Wrap and Aspen's Spaceloft. The blankets were tested, each at a time, by installing them in panel 1 (aerogel panel). The first set tested was Cabot's Thermal Wrap (set 1) and the second set tested was Aspen's Spaceloft (set 2). Panel 3 (polyester insulation panel) was outfitted with a polyester insulation board and panel 2 (control panel) was left with a 6 mm air gap to serve as the control. The data collected for each panel included surface temperatures as detailed in section 4.6 and heat fluxes as detailed in section 4.7. These measurements were

analyzed to evaluate and compare the thermal performances of the blankets. Panel setup is explained in greater detail in section 4.5.

5.2.1. Cabot's Thermal Wrap

Fig. 32 represents the heat flux through aerogel panel, control panel, and polyester insulation panel over a period of 72 hours. The peak was the point at which heat flux and temperature readings were a maximum over a given day. Typically, the peaks for the exterior surface temperature occurred at around 2 PM and the peaks for heat fluxes as measured on the interior surface occurred at around 4 PM.

In Fig. 32, aerogel panel displayed a reduction in heat fluxes at their peaks of 24%, 20%, and 23% for peaks D1, D2, and D3 against control panel, respectively. This demonstrated consistency in performance, especially when considering that that outdoor air temperatures and exterior surface temperatures were less than 3 °C apart on the three consecutive days (Fig. 35). In Fig. 35, surface and ambient air temperatures are only shown for one panel (aerogel panel) because temperature readings from all three panels were identical. Polyester insulation panel displayed a reduction in heat fluxes at their peaks of 17%, 15%, and 10% for peaks D1, D2, and D3 against control panel, respectively. Aerogel panel when compared with the polyester insulation panel displayed a reduction in heat fluxes at their peaks of 8%, 5%, and 14% for peaks D1, D2, and D3, respectively. This is approximately a 9% reduction in heat flux of aerogel panel when compared to polyester insulation panel.

A reduction in the amplitude of heat fluxes passing through the panels signifies a reduced load on the chillers. This is particularly important because of the way in which

electric companies charge for electricity. Electric utility companies charge for energy consumption in kilowatt-hour for a fixed period, typically a month, and for a maximum monthly demand, in kilowatt, over a specific time interval, generally 15 minutes [52]. Reduction of the daily maximum amplitude can significantly reduce costs by decreasing the monthly demand.

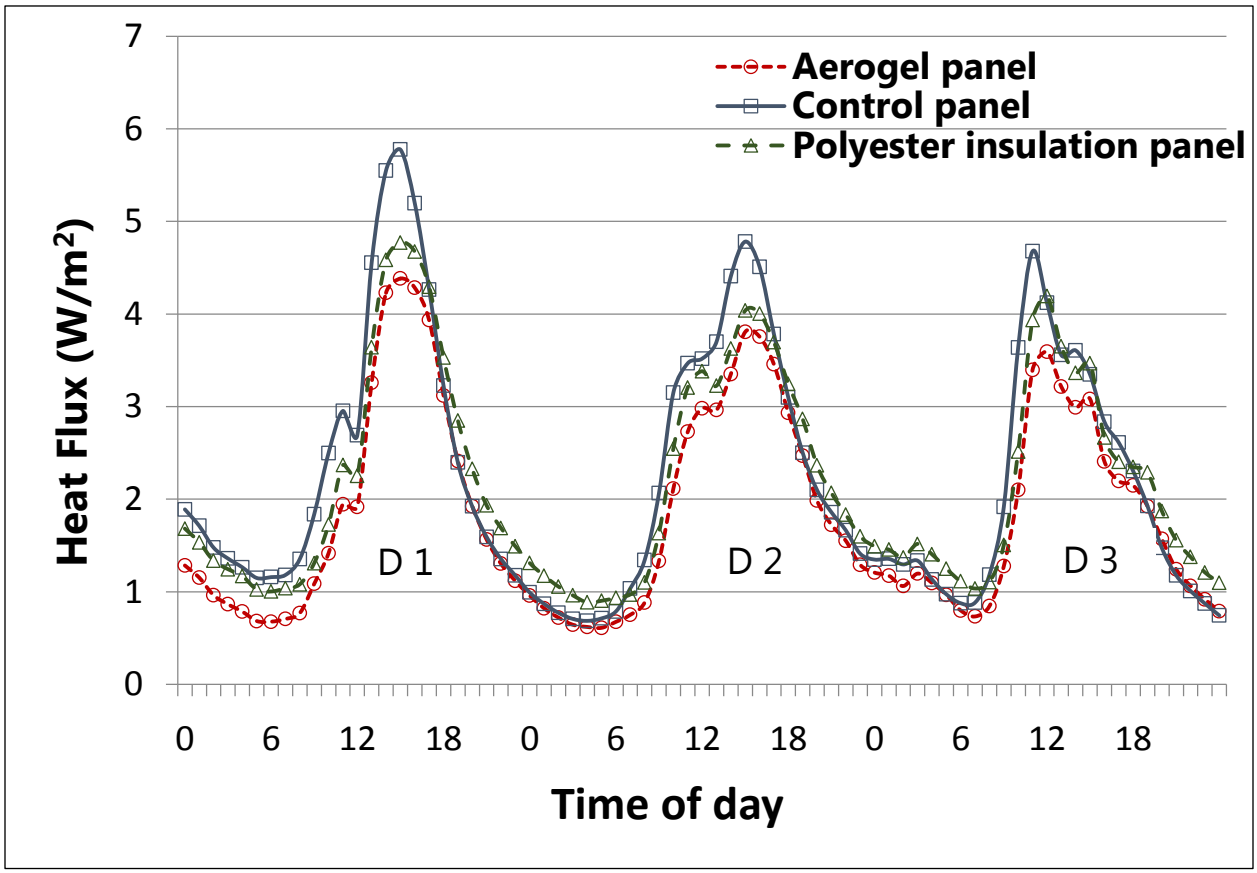

Fig. 32. Heat fluxes through the panels for set 1.

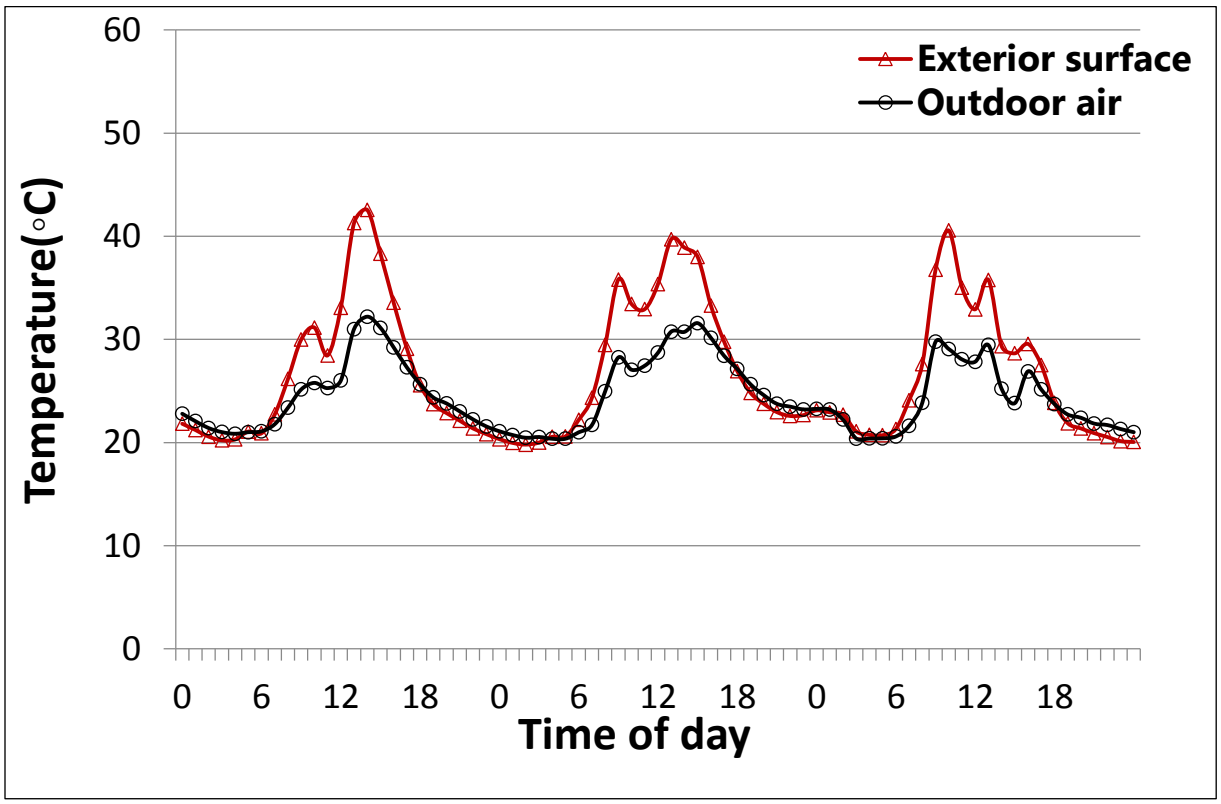

Fig. 33. Outdoor air and exterior surface temperatures for set 1.

To get a more thorough quantification of the blankets thermal performance, the daily heat transfer across the panels was calculated. This is the area under the heat flux curve for a given day (Fig. 32). The reductions in daily heat flows for the aerogel panel were 23%, 16%, and 15% for days D1, D2, and D3 when compared with the control panel, respectively. Therefore, the aerogel panel was found to perform with an 18% average reduction in daily heat flows when compared to the control panel. The reductions in heat fluxes for the polyester insulation panel were 8%, 2%, and -1% for days D1, D2, and D3 when compared with the control panel, respectively. The polyester insulation panel showed an average reduction of 3% in daily heat flow when compared to the control panel. The reductions in daily heat flows for the aerogel panel were 16%,

14%, and 16% for days D1, D2, and D3 when compared with the polyester insulation panel, respectively. Therefore, the aerogel panel performed with a 15% reduction in heat flow when compared to the polyester insulation panel.

In Table 8, temperatures inside the air space are shown, namely air space panel surface temperatures and cement board surface temperatures. This was done to indicate the reductions in the amplitudes of the surface temperatures in locations just before and after the insulations were applied.

Table 8
Panel air space temperatures for set 1.

	Air space panel surface (°C)			**Difference (°C)**			**Air space cement board surface (°C)**		
	Aerogel panel	Control panel	Polyester insulation panel	Aerogel Panel	Control panel	Polyester insulation panel	Aerogel panel	Control panel	Polyester insulation panel
Average	22.56	22.51	22.72	0.82	0.40	0.48	21.73	22.11	22.23
Maximum	26.14	25.44	25.98	2.39	1.21	1.77	23.75	24.23	24.21
Minimum	20.74	20.97	21.06	0.09	0.00	-0.14	20.65	20.97	21.21
Amplitude	5.40	4.47	4.91	2.30	1.21	1.91	3.10	3.27	3.01

It was inferred from Table 8 that using the aerogel blanket would reduce indoor surface temperatures. The difference in amplitudes of temperatures (maximum-minimum) between the air space panel surface and the air space cement board for aerogel panel, control panel, and polyester insulation panel were 2.30 °C, 1.21°C, and 1.91°C, respectively. For the aerogel blanket, this is an average temperature reduction of 0.82 °C when compared to the polyester insulation panel. The reductions seen at the minimums were less than 0.1 °C. This is not to say that the insulation was less effective at lower temperatures. Rather, at minimum temperatures outdoor and indoor air

temperatures were similar which prevented a significant temperature gradient from occurring. At maximum temperatures, while comparing the temperature differences across the air space panel, aerogel panel, control panel, and polyester insulation panel showed differences in temperatures of 2.39 °C, 1.21 °C, and 1.77 °C, respectively. This reduction in temperature changes helps maintain a constant interior surface temperature [53].

Fig. 34 shows the trends seen between indoor air temperature and interior surface temperatures.

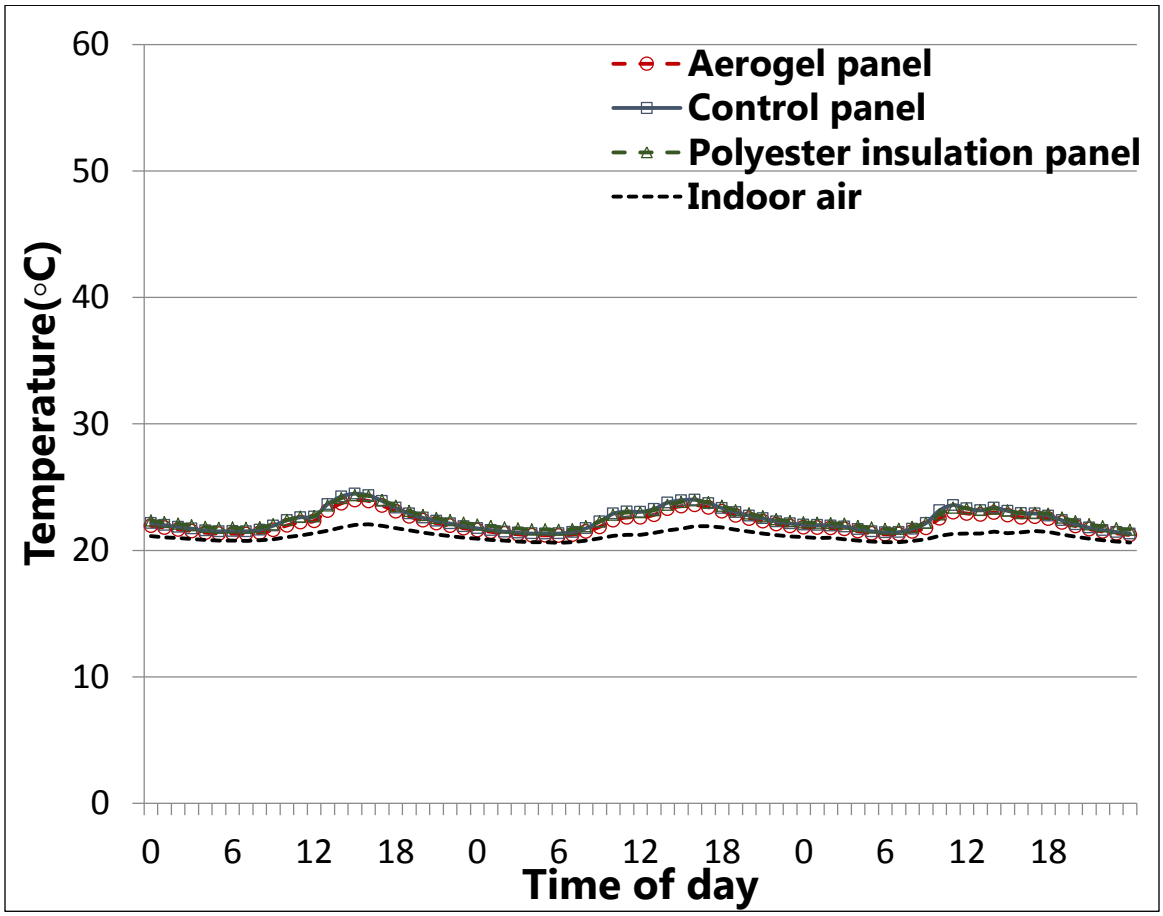

Fig. 34. Indoor air and interior surface temperatures for set 1.

The maximum interior surface temperatures for aerogel panel, control panel, and polyester insulation panel were 23.97°C, 24.48°C, and 24.35°C, respectively. The average air temperature recorded for the same period was 21.16 °C. Thermal discomfort occurs when the difference in indoor air temperature and interior wall temperature exceeds 3 °C [54]. This effect is more pronounced when subjects are standing closer to wall surfaces. The maximum panel temperatures for the control panel and the polyester insulation panel exceeded the 3 °C limit, whereas aerogel panel had a temperature difference of less than 3 °C against indoor air temperature. Moreover, it has been experimentally shown that thermal discomfort has an effect on human psychology and health. Persons working in an office environment, because of the perception of bad air quality (warm and/or humid air) performed tasks less efficiently [55].

Some electric companies also charge for power factors less than 0.95. A power factor is calculated by dividing real power (kW) by apparent power (kVA). This increase in apparent power is caused by induction motors such as the ones that are typically used to run air handlers and chiller units when they are lightly loaded instead of switched off. Reductions in the fluctuation of indoor wall temperatures allow the air-conditioning systems to turn off which prevents a reduction in power factor.

Fig. 35 indicates the performance of the panels in terms of daily heat flows and peak heat fluxes. In Fig. 35, aerogel panel, control panel, and polyester insulation panel are compared against each other. It was observed that the aerogel panel had larger reductions in both daily heat flow and heat flux when compared to the polyester insulation panel.

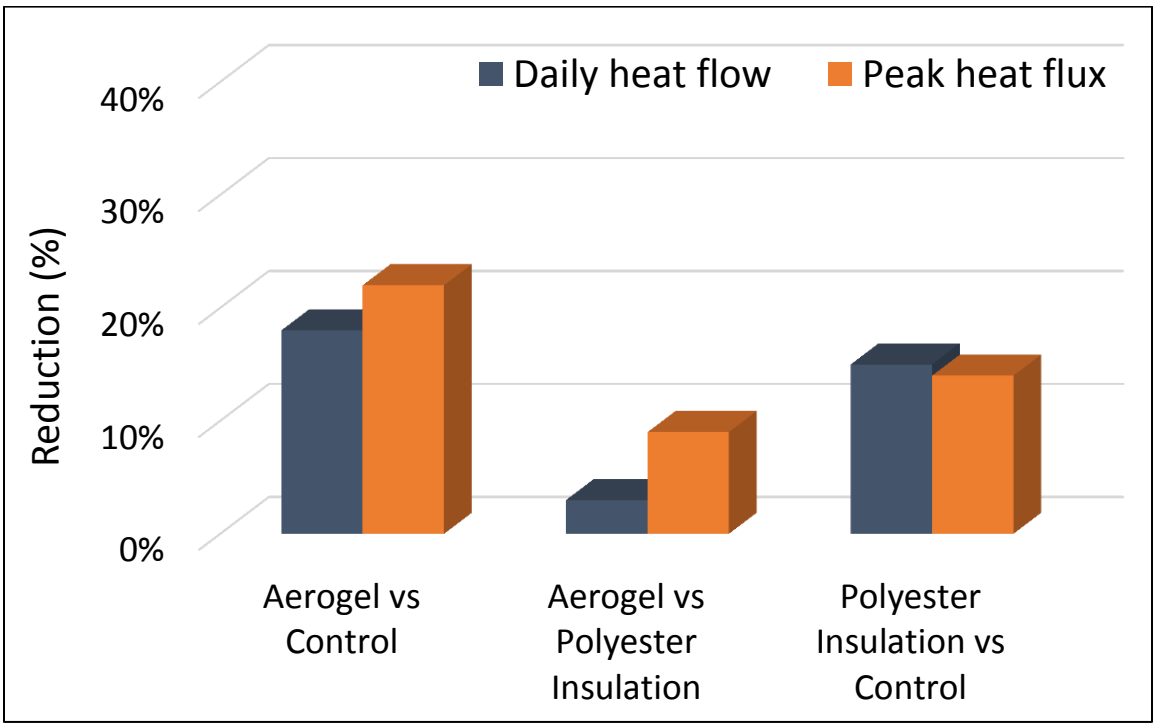

Fig. 35. Comparison of panel performances for set 1.

5.2.2. Aspen's Spaceloft blanket

Fig. 36 represents the heat flux through aerogel panel, control panel, and polyester insulation panel over a period of 72 hours. The peak was the point at which heat flux and temperature readings were a maximum over a given day. Typically, the peaks for the exterior surface temperature occurred at around 4 PM and the peaks for heat fluxes as measured on the interior surface occurred at around 5PM.

In Fig. 36, aerogel panel displayed a reduction in heat fluxes at their peaks of 16%, 16%, and 22% for peaks D1, D2, and D3 against control panel, respectively. This demonstrated consistency in performance. Polyester insulation panel displayed a reduction in heat fluxes at their peaks of 12%, 16%, and 22% for peaks D1, D2, and D3 against control panel, respectively. Aerogel panel when compared with polyester

insulation panel displayed a reduction in heat fluxes at their peaks of 4%, for peak D1 and showed a reduction of less than 1% for D2, and D3, respectively. This blanket did not show a significant reduction in heat flux at the peaks. In Fig. 37 exterior surface and ambient air temperatures are shown for all panels. Exterior surface temperatures were identical and well matched which implies that the panels were exposed to similar thermal conditions. Also, they followed trends that the outdoor air temperatures exhibited.

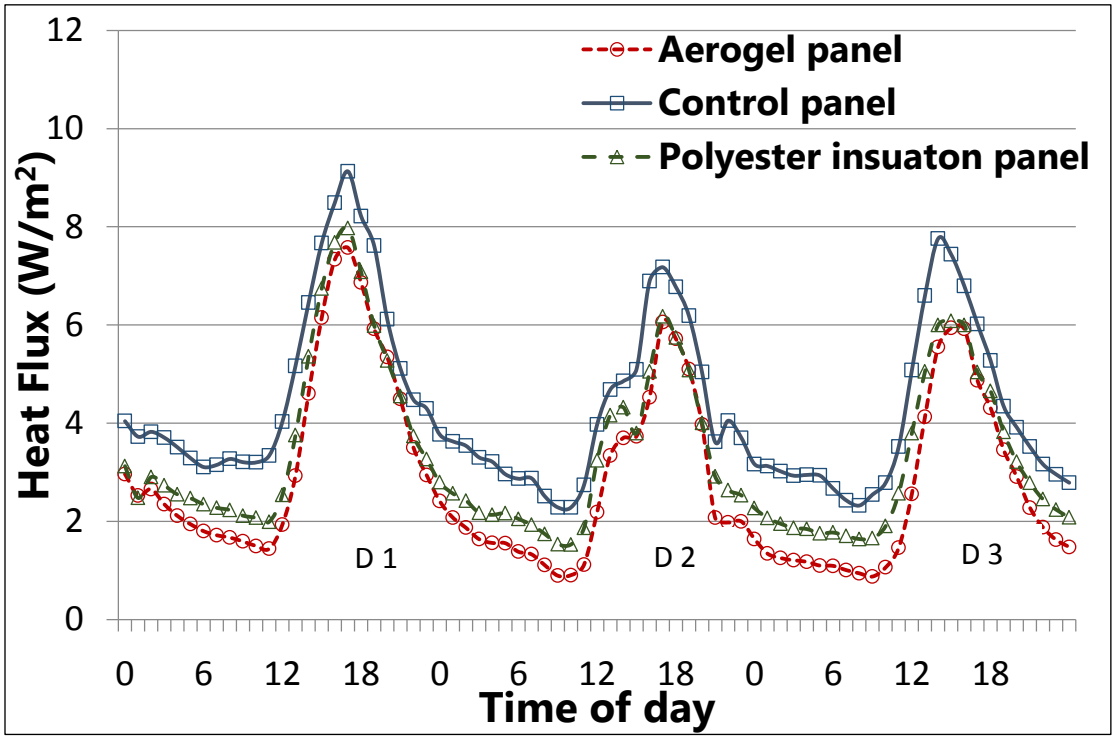

Fig. 36. Heat fluxes through the panels for set 2.

To get a more thorough quantification of the blankets thermal performance, the daily heat transfer across the panels was calculated. This is the area under the heat flux curve for a given day (Fig. 36). The reductions in daily heat flows for the aerogel panel were 29%, 37%, and 39% for days D1, D2, and D3 when compared with the control

panel, respectively. The aerogel panel showed a 35% average reduction in daily heat flow when compared to the heat flux across the control panel. For days D2 and D3, heat fluxes across the panels were similar and showed a similar reduction in daily heat flows. The reductions in daily heat flows for the polyester insulation panel were 21%, 24%, and 24% for days D1, D2, and D3 when compared with the control panel, respectively. The polyester insulation panel showed an average reduction of 23% in daily heat flow when compared with the control panel. The reductions in daily heat flows for the aerogel panel were 10%, 17%, and 29% for days D1, D2, and D3 when compared with the polyester insulation panel, respectively. Therefore, the aerogel panel performed with a 16% reduction in daily heat flow when compared with the polyester insulation panel.

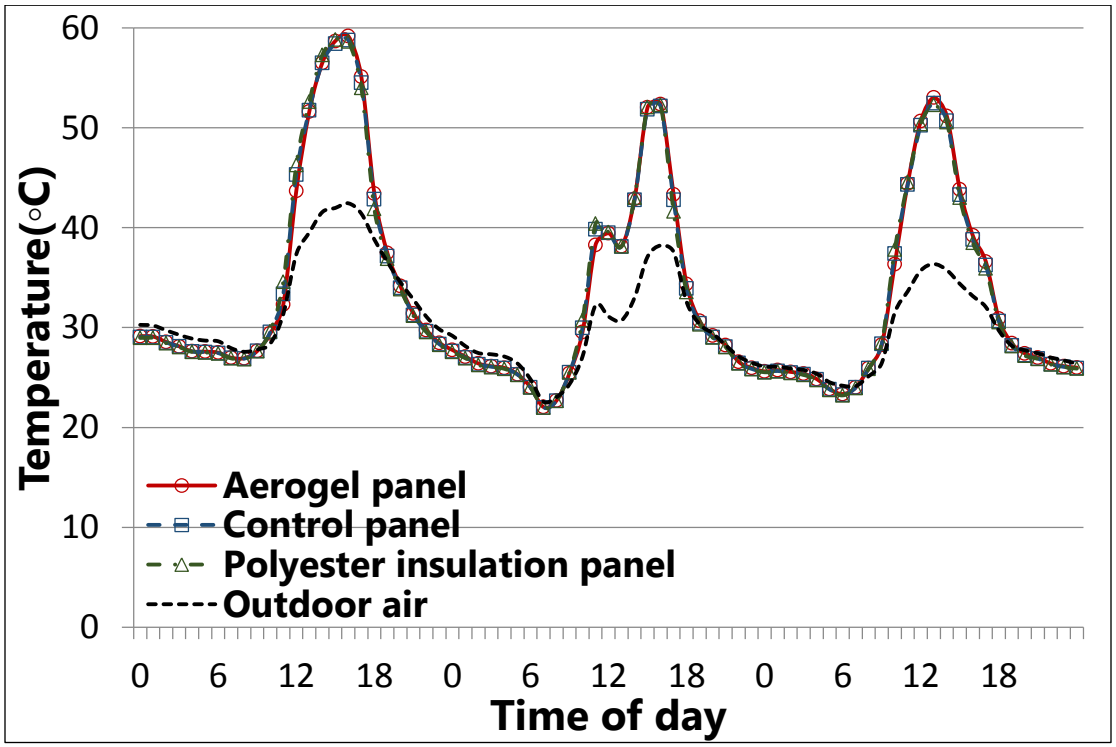

Fig. 37. Outdoor air and exterior surface temperatures for set 2.

It can be observed that the aerogel panel did not show significant heat flux reductions at the peaks. Rather, most of the reductions were seen during the off- peak intensities. To analyze these phenomena air space panel surface temperatures were examined (Fig. 38). On visual inspection of the graph, it is noticeable that the air space panel surface temperatures were higher for aerogel panel than control panel and polyester insulation panel.

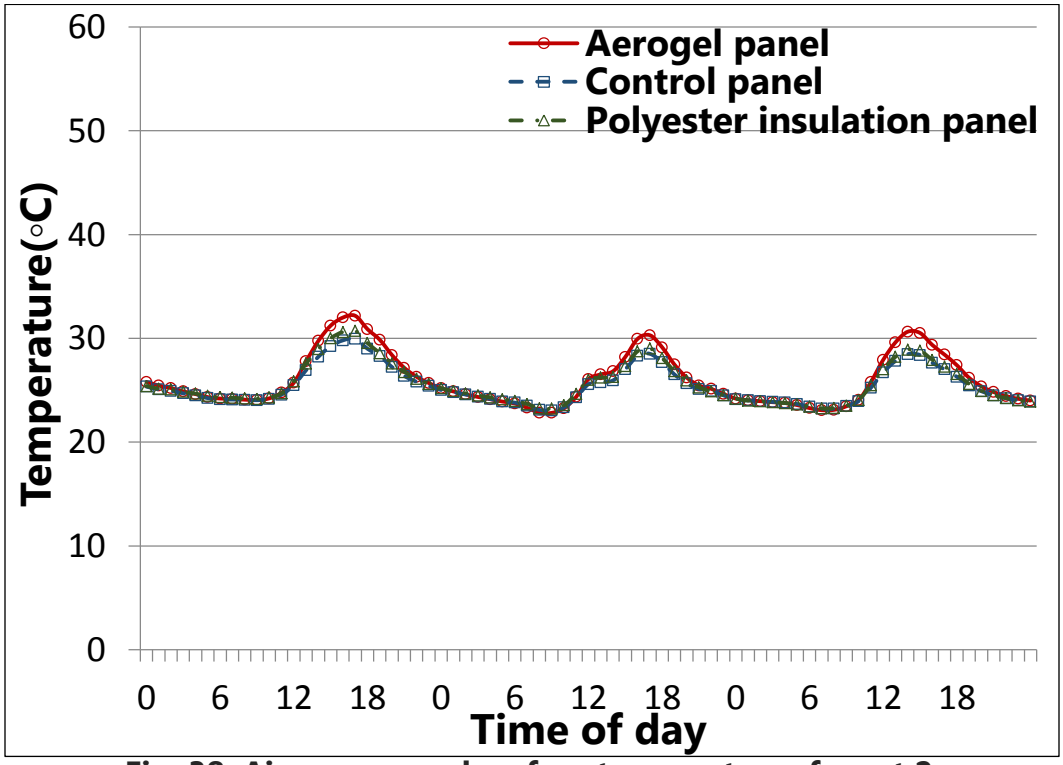

Fig. 38. Air space panel surface temperatures for set 2.

Table 9 tabulates the maximum air space surface temperatures for the air space panel surface and the air space cement board surface.

Table 9
Comparison of panel air space temperatures for set 2.

Panel surface	Aerogel panel (° C)	Difference (° C)	Control panel (° C)	Difference (° C)	Polyester insulation panel (° C)
Air space panel surface	32.18	-2.22	29.96	-0.76	30.72
Air space cement surface	27.25	-0.30	27.55	0.21	27.34

The temperatures of the air space panel surface were higher for both aerogel panel and polyester insulation panel when compared to control panel. This is expected considering that there exists a thermal resistance at the interface between the panels and the insulations. However, these differences were 2.22 °C for aerogel panel and 0.76 °C for polyester insulation panel when compared to the control panel. Aspen's Spaceloft blanket had its dust mixture (i.e., silica aerogel, calcium silicate, and synthetic graphite) coated between the fiber layers and also on the exterior surfaces as opposed to Cabot's Thermal Wrap that contained aerogel crystals held between fibers (Fig. 9, 11, and 12). This exterior coated dust layer provided a high thermal resistance to the thermal energy coming out of the air space panel surface at the interface itself. This thermal energy because of the difference between the exterior surface temperature and the air space panel surface temperature was stored at the interface. This raised air space panel surface temperatures in aerogel panel. Aerogel as explained in section 1.2.3 has higher thermal conductivities at higher temperatures. This increases the heat flux through aerogel panel as it reaches the peak for any given day. At off-peak times, namely between 10 PM to 10

AM, reductions in outdoor ambient and surface temperatures (Fig. 37) show a coinciding reduction in air space panel surface temperatures and subsequently heat flux through aerogel panel.

Fig. 39 indicates the performance of the panels in terms of daily heat flows and peak heat fluxes. In Fig. 39, aerogel panel, control panel, and polyester insulation panel were compared against each other. It was observed that the aerogel blanket had larger reductions in both daily heat flow and peak heat flux when compared to the polyester insulation board. This aerogel blanket showed a noticeably larger reduction in daily heat flow when compared to its peak heat flux.

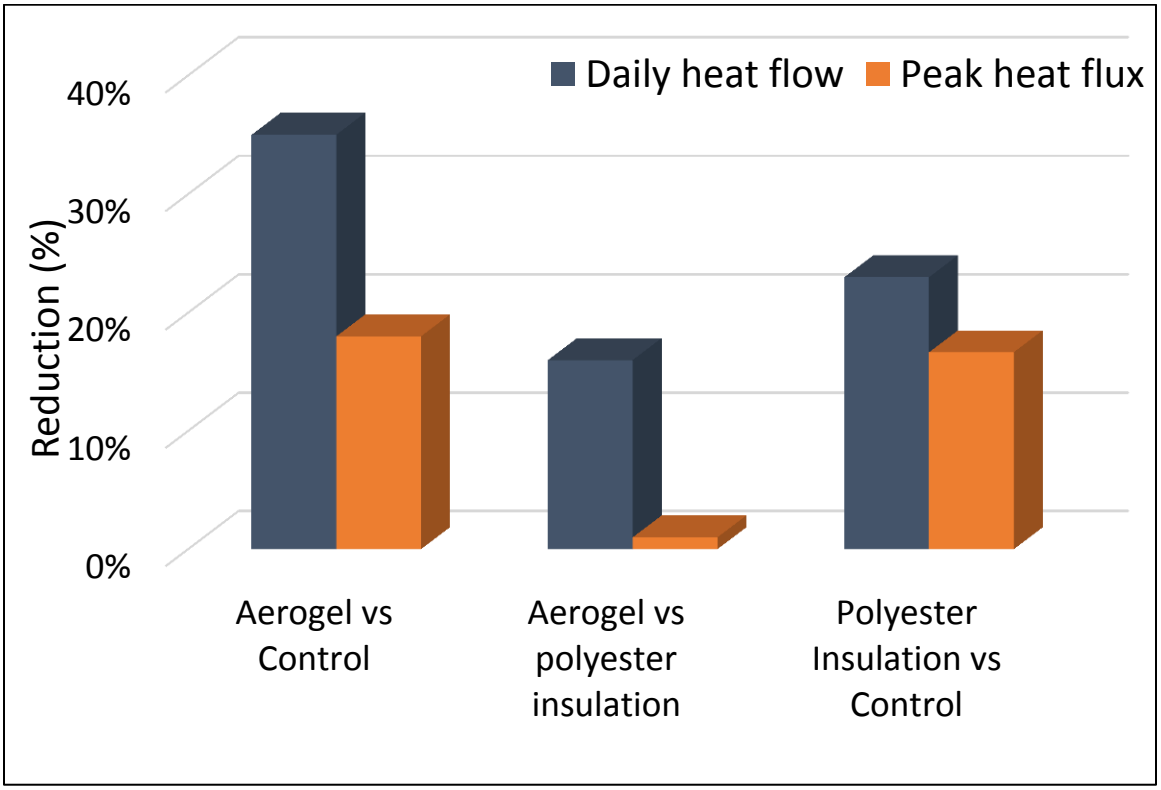

Fig. 39. Comparison of panel performances for set 2.

To compare the thermal performance of Cabot's Thermal Wrap and Aspen's Spaceloft their average thermal performances at the daily peaks and their respective daily heat transfer were tabulated in Table 10.

Table 10
Insulating blankets performance during retrofit test.

Insulating Blanket	**Control panel**		**Polyester insulation panel**	
	Peak	**Daily**	**Peak**	**Daily**
Cabot's Thermal Wrap	22%	18%	9%	15%
Aspen's Spaceloft	18%	35%	1%	16%

The blanket's thermal performance at lower temperatures is assumed to follow a linear distribution with respect to increased insulation thickness [56]. This implies that for a 6 mm blanket of Aspen's Spaceloft the reduction in daily heat flow when compared to the polyester insulation board would be closer to 19%. This heat flow reduction is 26% more than that Cabot's Thermal Wrap against the polyester insulation board. However, a larger reduction than seen was expected. This is because Aspen's Spaceloft contained approximately 27% more aerogel dust when compared with Cabot's Thermal wrap. Furthermore, it also contained calcium silicate and synthetic graphite which are both thermal insulators. The aerogel blankets showed only a marginal increase in performance when compared with the polyester insulation board.

Figs. 40 and 41 represent the R-value of the panels fitted with Cabot's Thermal Wrap and Aspen's Spaceloft over a 72 hour period.

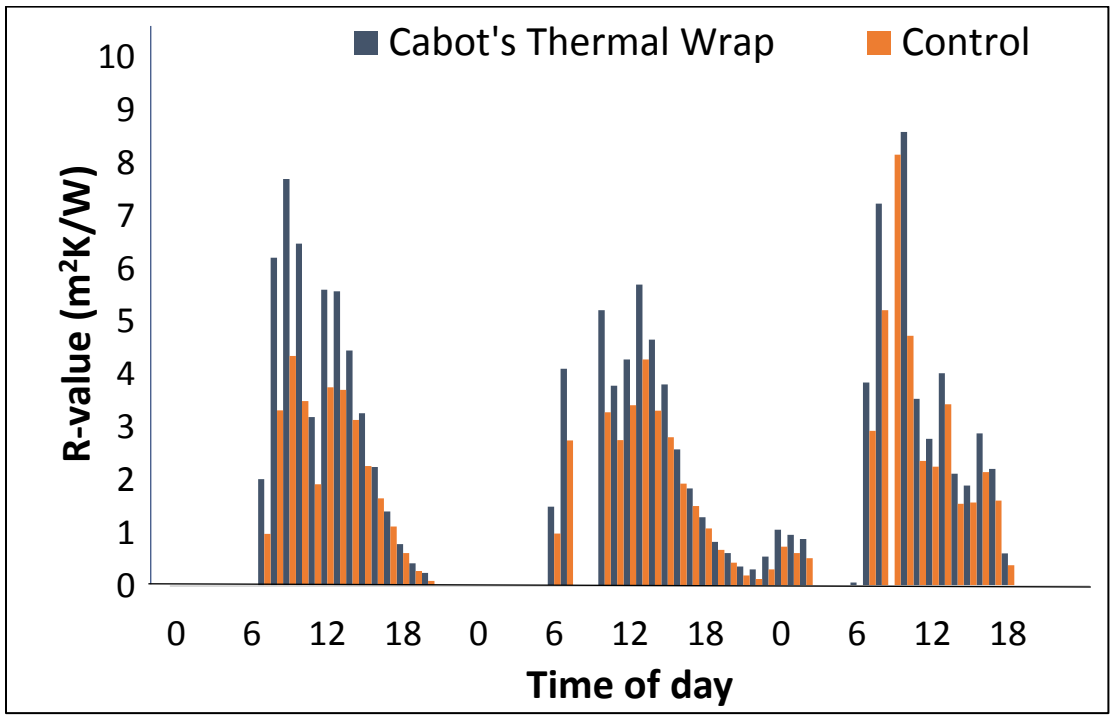

Fig. 40. R-value of panel fitted with Cabot's Thermal Wrap.

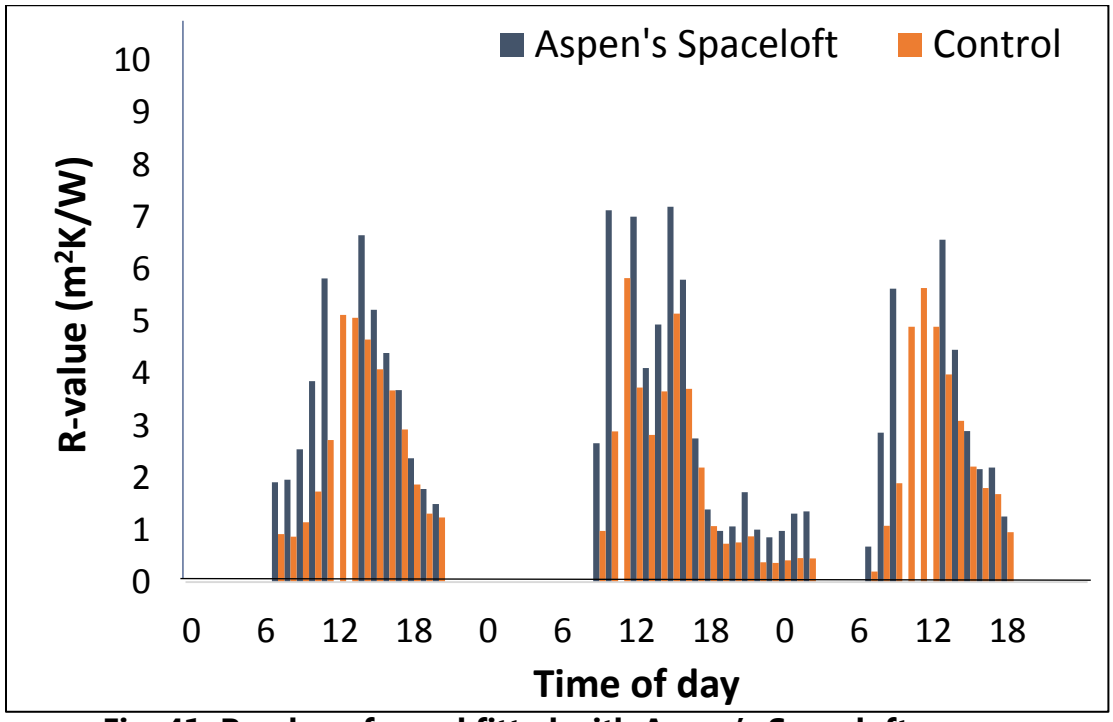

Fig. 41. R-value of panel fitted with Aspen's Spaceloft.

In Figs. 40 and 41, the R-values were an average of 2.37 m^2K/W and 2.41 m^2K/W for the control panels, respectively. This reiterated the level of accuracy that was maintained throughout the experiment and made the R-values of Cabot's Thermal Wrap and Aspen's Spaceloft more comparable. The panel fitted with Cabot's Thermal Wrap was found to have an average R-value of 2.97 m^2K/W. The panel fitted with Aspen's Spaceloft had an average R-value of 3.22 m^2K/W. This showed that Cabot's Thermal Wrap had a lower R-value than Aspen's Spaceloft. Aspen's Spaceloft was expected to have a higher R-value based on the quantitative analysis. However, as mentioned earlier its R-value is not as high as was expected.

Furthermore, the R-value and thermal conductivity of the blankets was compared with the R-value and thermal conductivity of an aerogel monolith. This was done by relating the thermal conductivity, R-value, and peak heat flux of the air space in the control panel with the thermal conductivity, R-value, and heat flux of the blanket in aerogel panel. All the panels showed similar interior and exterior temperatures, i.e., the driving force for the incoming heat flux. For this reason, temperature differences were considered to be constant.

A 6 mm air gap has an R-value of 0.23 m^2K/W or a thermal conductivity of 0.026 W/mK. The R-value of the blankets were a minimum at peak heat fluxes (Figs. 32, 36, 40, and 41). At the peak heat flux, the blankets showed a minimum heat flux reduction of 16% when compared to the control panel. This implied that the R-value of the blankets reached values of approximately 0.28 m^2K/W or a thermal conductivity of 0.021 W/mK. The highest peak heat flux reduction was 24%. This means that the highest R-value achieved by the blankets were approximately 0.31 m^2K/W or a thermal conductivity of

0.019 W/mK. Typical R-values for an equivalent sized silica aerogel monolith is 0.35 m^2K/W and a thermal conductivity of 0.017 W/mK [11]. This difference in R-value showed that the aerogel blankets did not have the same thermal performance as an aerogel monolith.

To investigate this, the infrared wavelength at which maximum radiation occurs was calculated using Wien's displacement law shown in Eq. (5.1).

$$\lambda_{MAX} = \frac{2897\mu m°K}{T} \tag{5.1}$$

In aerogels, radiation is a dominant mode of heat transfer; thus the need to quantify the wavelength of infrared radiation to which the aerogel dust was exposed to. This in turn provides an interpretation of the extinction coefficient of the aerogel dust (refer to section 1.2.3). λ_{MAX} was found to be between 9-10 μm for both the blankets tested. At these wavelengths silica aerogel has a high attenuation which absorbs thermal radiation and dissipates it. Therefore, the wavelength of emitted infrared waves was not the cause for the underperformance of Aspen's Spaceloft. The size of the dust particles in Aspen's Spaceloft meant that it was more likely to adhere to the fiber glass and polyethylene fibers than to be trapped in between fibers as was the case in Cabot's thermal wrap (Fig. 12). Radiative fluxes at the boundary of aerogel dust are weak as a result of lower boundary emissivity. Heat travels in and out of aerogel mostly through conduction. The heat flux through the aerogel body is governed by conduction and radiation. This difference in modes of heat transfer at the boundary and at the interior creates an unusual temperature profile in which the slope for the exterior of the aerogel is far

steeper than the interior [16,23]. Based on Fourier's law, because of the sudden changes in temperatures at the boundary, the rate of heat transfer is higher. The contact between the aerogel dust and fibers provides a thermal pathway for heat to leave the aerogel dust particles, which enhances the thermal conductivity of the composition. Furthermore, smaller aerogel dust particles result in faster transition periods for heat fluxes.

Having smaller aerogel dust particles is not necessarily less effective provided they are in close contact to one another behaving much like a monolith. Gao et al. [57] showed that smaller particles (<0.5 mm) that are all in close contact have a lower thermal conductivity than larger particles (3–5 mm). This is because of a reduction in inter-spatial voids of the aerogel composition. This, however, is not the case with aerogel blankets (Figs. 9, and 11). Fig. 42 is used to illustrate.

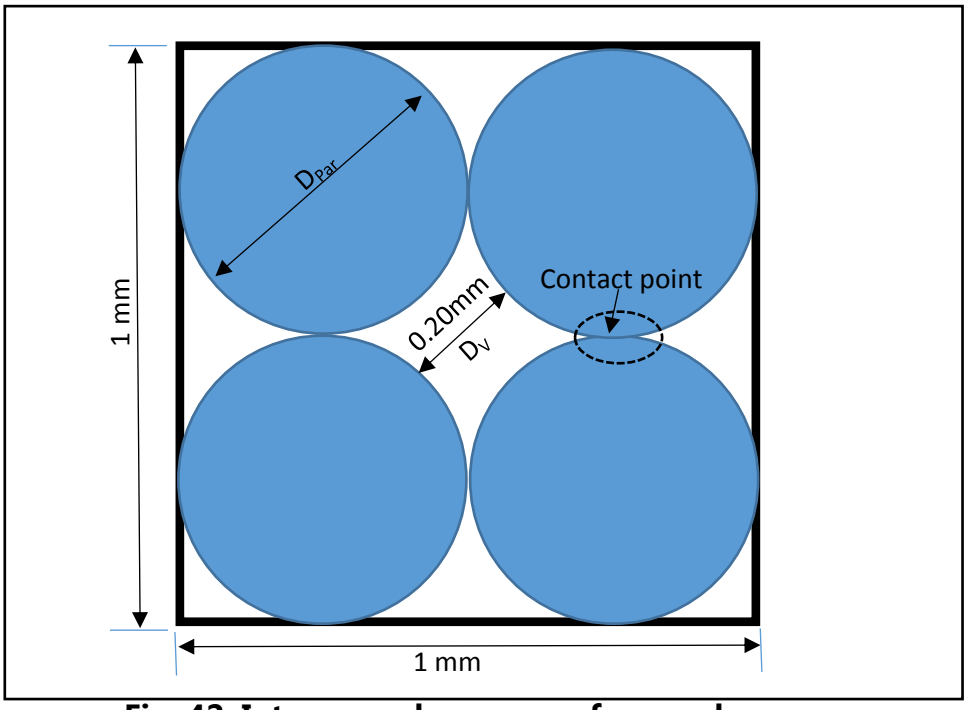

Fig. 42. Inter-granular spaces of aerogel.

In Fig. 42, the aerogel granules were approximated as circles of diameter of 0.5 mm and the rhombus in the center represented the interspatial voids that are formed. This inter-granular distance can be estimated using Eq. (5.2).

$$\mathrm{D_V} = \frac{12}{29} D_{Par} \tag{5.2}$$

For a particle diameter size (D_{Par}) of 0.5 mm the minimum inter-granular distance (Dv) was calculated as 0.20 mm. The objective in using a composite is to minimize this interspatial void so as to prevent convective flows and minimize gaseous conductivity. This can be achieved by using smaller aerogel granules that can be more densely packed. To achieve the highest packing density a mixture of different granule sizes are

preferred. These smaller particles can fill in larger interspatial voids. Preferably, air voids should be less than the mean free path of air (~700 nm) which would effectively reduce gaseous conductivity. In the case shown in Fig. 42 granules smaller than 0.20 mm would reduce gaseous conductivity and convection. Moreover, an increase in the number of granules will increase the number of thermal contact resistances for a given volume.

It has been shown previously by using aerogel granules that are in contact with one another and are densely packed within a medium result in a thermal behavior that was similar to an aerogel monolith. This method has been used effectively to make aerogel glazed units to achieve lower thermal conductivities and is commercially available.

Chapter 6
Conclusions and recommendations

6.1. Research summary

The purpose of this research was to study and to test the effectiveness of aerogel used in blanket form as a potential next generation thermal insulation. This implied understanding and analyzing the thermal mechanisms that allowed aerogel to have low thermal conductivities and to observe if these mechanisms were sustained when aerogel was used in a dispersed form (Non-monolithic). Aerogel was integrated into part of one wall of the building enclosure of an institutional building (M2SEC) by the use of thin polymer blankets (<6 mm) that behaved as containment vehicles for the aerogel dust particles. Two blankets were tested. They were Cabot's Thermal Wrap and Aspen's Spaceloft which were both silica based aerogel blankets. A number of characterization tests were carried out on the aerogel to support the thermal analysis of the aerogel blankets. These tests include scanning electron microscopy, energy-dispersive X-ray spectroscopy, and quantitative analyses.

A total of three sets of data were collected, namely pre-retrofit test or calibration test, Cabot's Thermal Wrap test, and Aspen's Spaceloft test. Calibration tests were carried out on three test panels that were located in the south wall of the M2SEC research building to confirm equal thermal performance between them and to provide the baseline for their comparison. The blankets were applied, one at a time, to the M2SEC building wall via interchangeable panels for experimental evaluation.

6.2. Conclusions

The data from the calibration test showed a high degree of similarity between the thermal performances of the panels. For the exterior surface temperatures and the outdoor ambient air temperatures the differences in temperatures between the panels were less than 0.03 °C. The exterior temperature and solar irradiance were the driving forces for the heat fluxes that entered the building. Heat flux entering the building had an average difference of 4.2% between the panels. Moreover, indoor air temperatures were maintained at a difference of less than 0.17 °C. This high level of control ensured that data collected during the retrofit was accurate.

The experiments concluded that aerogel blankets reduced peak heat fluxes by approximately 22% and daily heat flows by about 35% when compared to wall panels without aerogel. When the aerogel blankets were compared against conventional insulation (polyester insulation boards) it showed a peak reduction of about 9% and a daily heat flow reduction of less than 16% (Table 10). This reduction was less than what is expected from monolithic silica aerogels and showed marginal improvement when compared to the polyester insulation board.

The analysis indicated that the aerogel dust of both blankets was similar in pore size. This was important because pore size is a crucial factor in the thermal mechanisms of aerogels. Aerogel blankets differ widely in composition and manufacturing. For the blankets that were tested the crucial differences were:

1) The dust in Cabot's Thermal Wrap contained only aerogel, whereas, the dust in Aspen's Spaceloft contained aerogel, synthetic graphite, and calcium silicate.

2) The average size of the aerogel dust particles was larger and more varied for Cabot's Thermal Wrap (< 500 μm) than for Aspen's Spaceloft (<100 μm).
3) The quantity of aerogel dust was greater in Aspen's Spaceloft than in Cabot's Thermal Wrap on the basis of volume.

It has been proven in a large number of research publications that silica aerogels have a low thermal conductivity. The issue is how to transfer this low thermal conductivity into building enclosures via a containment method while keeping in mind economic factors.

The thermal mechanisms that have been mathematically modelled for aerogels cannot be used to map thermal pathways for this heterogeneous composition (aerogel blankets); therefore, more research is needed in this area. By comparing the differences in composition and structure of both the blankets the following conclusions were made:

1) Size and volume of aerogel particles used in aerogel blankets play a major role in its thermal performance.
2) Aerogel blankets tested were not as effective as aerogel monoliths.
3) The blankets showed marginal reductions in heat flux when compared to the polyester insulation board.
4) Aerogels blankets perform better at lower temperatures.

6.3. Recommendations

Aerogel blankets tested cannot be expected to have similar thermal performances as aerogel monoliths as their aerogel content was less than half and moreover in a dispersed form. The key to aerogels effectiveness as thermal insulator is its nanopore structure. It is crucial that a synthesis with any type of containment method creates macropores that are as small as possible. It is recommended that this method of aerogel application be investigated for wall insulations by using alternate containment methods that will reduce inter particular space. Optimization of packing density can be done by using established Euclidian geometry and circle packing principles. This should be experimentally tested and optimized. Furthermore, xonotlite-type calcium silicate (<100 nm) can be used as filler in the composite. The xonotlite-aerogel composite has been shown to have similar thermal trends to aerogels. This may prove more economical.

As mentioned in section 5.2.2, at the surface of aerogel, conduction is a significant mode of heat transfer for heat entering and leaving the aerogel particles when compared with convection and radiation. For this reason, it is recommended that aerogel blankets be tested while maintaining an airspace between the blanket and the surface conducting heat. Moreover, it would prevent accumulation of heat at the composite-panel interface.

Future research should focus on mathematically modelling the thermal interactions between aerogel and its supporting fibers because aerogels behave differently when in contact with other materials. For example, this would help optimize

aerogel dust and fiber diameters that may lead to lower thermal conductivities. Testing should also be conducted during the winter to conclusively determine and map the thermal performance of aerogel blankets. Furthermore, seasonal sets of data can help show agreement between the thermal model and experimental data or be used on extrapolation to mathematically model its thermal behavior.

REFERENCES

1] The U.S Energy Information Administration (EIA), Internal energy outlook 2013, http://www.eia.gov/forecasts/ieo/world.cfm (accessed 19.01.2014)

2] World Energy Council, World Energy Resources 2013 Survey, http://www.worldenergy.org/wp-content/uploads/2013/09/Complete_WER_2013_Survey.pdf (accessed 19.01.2014)

3] Knoema, World reserves of fossil fuels, http://knoema.com/smsfgud/world-reserves-of-fossil-fuels (accessed 19.01.2014)

4] National Resource Defense Council, Extreme Weather: Impacts of Climate Change, http://www.nrdc.org/globalwarming/climate-change-impacts/ (accessed 19.01.2014)

5] International Energy Agency, Technology Roadmap: Energy-efficient Buildings: Heating and Cooling Equipment (Insights), http://www.iea.org/publications/freepublications/publication/name,3984,en.html (accessed 19.01.2014)

6] M. A. Aegerter, N. Leventis, M. M. Koebel, Aerogels Handbook, Advances in Sol-Gel Derived Materials and Technologies, Springer (2011).

7] M. S. Al-Homoud, Performance characteristics and practical applications of common building thermal insulation materials, Building and Environment 40 (2005) 353–366.

8] T. Thorsell, Advances in Thermal Insulation - Vacuum Insulation Panels and Thermal Efficiency to Reduce Energy Usage in Buildings, KTH Royal Institute of Technology, 2012.

9] B. P. Jelle, Traditional, state-of-the-art and future thermal building insulation materials and solutions – Properties, requirements and possibilities, Energy and Buildings 43 (2011) 2549–2563.

10] R. Baetens, B. P. Jelle, A. Gustavsend, Aerogel insulation for building applications: A state-of-the-art review, Energy and Buildings 43 (2011) 761–769.

11] Aerogel.org, http://www.aerogel.org/ (accessed 16.6.2014)

12] J. L. Gurav, I. K. Jung, H. H. Park, E. S. Kang, and D. Y. Nadargi, Silica Aerogel: Synthesis and Applications, Journal of Nanomaterials (2010).

13] E.O. Lawrence Berkeley National Laboratory, Microstructured Materials Group, Silica AeroGels, http://energy.lbl.gov/ecs/aerogels/sa-chemistry.html (accessed 19.01.2014)

14] I. K. Jung, C-S. Park, T-J. Ha, H-H. Park, and S. Baek, 'Effect of surface modification of SiO_2 nanoparticles on the mechanical properties of ambient pressure dried silica

aerogels', International journal of Nanotechnology 10 (2010) 811–818.

15] M. Ayers, E.O. Lawrence Berkeley National Laboratory, http://www.aerogel.org/?p=416 (accessed 19.01.2014)

16] J. Fricke, T. Tillotson, Aerogels: production, characterization, and applications, Thin Solid Films 297 1–2 (1997) 212–223.

17] A. Hunt and M. Ayers, History of Silica Aerogels, Lawrence Berkeley National Laboratory, http://energy.lbl.gov/ecs/aerogels/ (accessed 19.01.2014)

18] A. C. Pierre and G. M. Pajonk, Chemistry of Aerogels and Their Applications, Chemical Reviews 102 (2002) 4243−4265.

19] Qi Tang, Tao Wang, Preparation of silica aerogel from rice hull ash by supercritical carbon dioxide drying, Journal of Supercritical Fluids 35 (2005) 91–94.

20] E.O. Lawrence Berkeley National Laboratory, Microstructured Materials Group,Silica AeroGels, http://energy.lbl.gov/ecs/aerogels/sa-making.html (accessed 19.01.2014).

21] A. S. Dorcheh, M. H. Abbasi, Silica aerogel; synthesis, properties and characterization, Journal of Materials Processing Technology 199 (2008) 1–3 10–26.

22] P. H Tewari, A. J. Hunt, K. D .Lofftus, Ambient-temperature supercritical drying of transparent silica aerogels, Materials Letters 9–10 (1985) 363–367.

23] X. Lu, R. Caps, J. Fricke, C. T. Alviso, R. W. Pekala, Correlation between structure and thermal conductivity of organic aerogels, Journal of Non-Crystalline Solids 188 (1995) 226-234.

24] D. W. Schaefer, K. D. Keefer, Structure of Random Porous Materials: Silica Aerogel, Physical Review Letters 56 (1998) 20.

25] J. Fricke, X. Lu, P. Wang, D. Buttner and U. Heinemann, International Journal of Heat Mass Transfer 35 (1992) 2305.

26] S. S. Kistler, The calculation of the surface area of microporous solids from measurements of heat conductivity, Journal of Physical Chemistry, 46 1 (1942) 19–31.

27] M. G. Kramer, Thermal insulation in Cryogenic Engineering, (Israel program for scientific translations, Jerusalem, 1969)

28] S. S. Kistler, The relationship between heat conductivity and structure in silica aerogel, Journal of Physics Chemistry, 39, 1 (1935) 79–86.

29] R. Caps, and J. Fricke, Radiative Heat Transfer in Silica Aerogel, First International Symposium on Aerogels (1st ISA). 1985. W€urzburg, Germany: Springer-Verlag.

30] U. Heinemann, R. Caps and J. Fricke, Radiation-conduction interaction: an investigation on silica aerogels, International journal of Heat and Mass Transfer 39 10 (1996) 2115-2130.

31] X. Lu, P. Wang, D. Buttner, U. Heinemann, O. Nilsson, J. Kuhn, and J. Fricke, Thermal transport in opacified monolithic silica aerogels, High Temperatures - High Pressures 23(4) (1991) 431–436.

32] R. Siegeland, and J.R. Howell, Thermal Radiation heat transfer, Tokyo: McGraw-Hill Kogakushka, Ltd (1972).

33] L.W. Hrubesh, Aerogel applications, Journal of Non-Crystalline Solids 225 (1998) 335–342.

34] Aerogel.org, Google Nexus 7 Body Made from Aerogel, http://www.aerogel.org/?p=2068 (accessed 10.5.2014).

35] M. Reim, A. Beck, W. Korner, R. Petricevic, M. Gloria, M. Weth,T. Schliermann, J. Fricke, C. H. Schmidt, and F. J. Potter, Highly insulating aerogel glazing for solar energy usage, Solar Energy 72 1 (2002) 21–29.

36] Y. Zhanga, R. Yanga, and R. Zhaoa, A model for analyzing the performance of photocatalytic air cleaner in removing volatile organic compounds, Atmospheric Environment 37 (2003) 3395.

37] U.S. Greenhouse Gas Abatement Mapping Initiative, McKinsey and Co. 2007, http://www.c2es.org/docUploads/US_ghg_final_report.pdf (accessed 19.01.2014).

38] J. Fricke, E. Hummer, H.-J. Morper, and P. Scheuerpflug, Thermal properties of silica aerogels, Journal of Applied Physics, 50 (1989) C487-C497.

39] L. W. Hrubesh, "Aerogels: The World' s Lightest Solids." ChemInform 22 (1991)13.

40] G. C. Ruben, L. W. Hrubesh, and T. M. Tillotson, High resolution transmission electron microscopy nanostructure of condensed-silica aerogels, Journal of Non-Crystalline Solids 186 (1995) 209-218.

41] S. T. Nguyen, Jingduo Feng, Shao Kai Ng, Janet P.W. Wong, Vincent B. C. Tan, and Hai M. Duong, Advanced thermal insulation and absorption properties of recycled cellulose aerogels Colloids and Surfaces A: Physicochem. Eng. Aspects 445 (2014) 128–134.

42] G. Carlson, D. Lewis, K. McKinley, J. Richardson, and T. Tillotson, Aerogel commercialization: technology, markets and costs Journal of Non-Crystalline Solids 186 (1995) 372-379.

43] D. M. Smith, Alok Maskara, and Ulrich Boes, Aerogel-based thermal insulation, Journal of Non-Crystalline Solids 225 (1998) 254–259.

44] E. Cuce, P. M. Cuce, C. J. Wood, and S. B. Riffat, Optimizing insulation thickness and analysing environmental impacts of aerogel-based thermal superinsulation in buildings, Energy and Buildings 77 (2014) 28–39.

45] S.Q. Zeng, A. Hunt, and R. Greif, Theoretical modeling of carbon content to minimize heat transfer in silica aerogel, Journal of Non-Crystalline Solids 186 (1995) 271-277.

46] Thermal and electrical conductivity of monolithic carbon aerogels, X. Lu, O. Nilsson, J. Fricke, and R. W. Pekala, Journal of Applied Physics 73 (1993) 581.

47] Cabot Corp., http://www.cabotcorp.com/wcm/download/enus/ae/ThermalWrap_350_600_800_DS_2013_v4_final%20lo%20res1.pdf (accessed 16.6.2014).

48] Aspen aerogels, http://www.starch.dk/private/energy/img/Spaceloft_DS.pdf (accessed 19.01.2014)

49] Aspen aerogels, http://www.aerogel.com/_resources/common/userfiles/file/Data%20Sheets/Spaceloft_MSDS.pdf (accessed 19.01.2014)

50] Y. Jiang, and Q. Chen, Effect of fluctuating wind direction on cross natural ventilation in buildings from large eddy simulation, Building and Environment 37 (2002) 379–386.

51] S. Holmberg, and Q. Chen, "Air flow and particle control with different ventilation systems in a classroom," Indoor Air 13 (2003) 200-204.

52] National Grid, http://www.nationalgridus.com/niagaramohawk/non_html/eff_elec-demand.pdf (accessed 19.01.2014)

53] J. F Straube, and E. F. P Burnett, Building science for building enclosures, Building science press (2005).

54] Saint-Gobain, http://www.isover.com/Our-commitment-to-sustainability/Comfort-and-well-being/Thermal-comfort (accessed 19.01.2014)

55] L. Lan, P. Wargocki, DP Wyon, and Z. Lian, Effects of thermal discomfort in an office on perceived air quality, SBS symptoms, physiological responses, and human performance, Indoor Air 21 (2011) 376–390.

56] M. Ozel, Thermal performance and optimum insulation thickness of building walls with different structure materials, Applied Thermal Engineering 31 (2011) 3854–3863.

57] T.Gao, B. P. Jelle, T. Ihara, and A. Gustavsen, Insulating glazing units with silica aerogel granules: The impact of particle size, Applied Energy 128 (2014) 27–34.